SANDIA REPORT

SAND2013-0512
Unlimited Release
Printed February 2013

Development of Advanced Strain Diagnostic Techniques for Reactor Environments

Darryn D. Fleming, Thomas V. Holschuh, Tim J. Miller, Aaron C. Hall,
David A. Urrea, Jr., Edward J. Parma

Prepared by
Sandia National Laboratories
Albuquerque, New Mexico 87185 and Livermore, California 94550

Sandia National Laboratories is a multi-program laboratory managed and operated by Sandia Corporation, a wholly owned subsidiary of Lockheed Martin Corporation, for the U.S. Department of Energy's National Nuclear Security Administration under contract DE-AC04-94AL85000.

Issued by Sandia National Laboratories, operated for the United States Department of Energy by Sandia Corporation.

Available to DOE and DOE contractors from
U.S. Department of Energy
Office of Scientific and Technical Information
P.O. Box 62
Oak Ridge, TN 37831

Telephone: (865) 576-8401
Facsimile: (865) 576-5728
E-Mail: reports@adonis.osti.gov
Online ordering: http://www.osti.gov/bridge

Available to the public from
U.S. Department of Commerce
National Technical Information Service
5285 Port Royal Rd.
Springfield, VA 22161

Telephone: (800) 553-6847
Facsimile: (703) 605-6900
E-Mail: orders@ntis.fedworld.gov
Online order: http://www.ntis.gov/help/ordermethods.asp?loc=7-4-0#online

SAND2013-0512
Unlimited Release
Printed January 2013

Development of Advanced Strain Diagnostic Techniques for Reactor Environments

Darryn D. Fleming, Thomas V. Holschuh
Advanced Nuclear Concepts

Tim J. Miller
Sensing and Imaging Technologies

Aaron C. Hall, David A. Urrea, Jr.
Multiscale Metallurgical S&T

Edward J. Parma
Applied Nuclear Technologies

Sandia National Laboratories
P.O. Box 5800
Albuquerque, New Mexico 87185-1130

Abstract

The following research is operated as a Laboratory Directed Research and Development (LDRD) initiative at Sandia National Laboratories. The long-term goals of the program include sophisticated diagnostics of advanced fuels testing for nuclear reactors for the Department of Energy (DOE) Gen IV program, with the future capability to provide real-time measurement of strain in fuel rod cladding during operation *in situ* at any research or power reactor in the United States. By quantifying the stress and strain in fuel rods, it is possible to significantly improve fuel rod design, and consequently, to improve the performance and lifetime of the cladding. During the past year of this program, two sets of experiments were performed: small-scale tests to ensure reliability of the gages, and reactor pulse experiments involving the most viable samples in the Annulated Core Research Reactor (ACRR), located onsite at Sandia. Strain measurement techniques that can provide useful data in the extreme environment of a nuclear reactor core are needed to characterize nuclear fuel rods. This report documents the progression of solutions to this issue that were explored for feasibility in FY12 at Sandia National Laboratories, Albuquerque, NM.

THIS PAGE INTENTIONALLY LEFT BLANK

1. CONTENTS

FIGURES

TABLES

NOMENCLATURE

ACRR	Annulated Core Research Reactor
AF	air flow
Al	aluminum
Al_2O_3	aluminum oxide
BCM	bridge completion module
DIC	Digital Image Correlation
DOE	Department of Energy
HPI	HiTec Products, Inc.
LDRD	Laboratory Directed Research and Development
LWR	light water reactor
Ni	nickel
NI	National Instruments
OFR	oxygen-to-fuel ratio
PFR	powder feed rate
PG	powder gas flow
SCFH	standard cubic feet per hour
SD	standoff distance
SEM	scanning electron microscope
SNL	Sandia National Laboratories
SS	stainless steel
TC	thermocouple
TF	total flow
VI	virtual instrument
V&V	Verification and Validation

1. INTRODUCTION

The following research was conducted as a Laboratory Directed Research and Development (LDRD) initiative at Sandia National Laboratories. The long-term goals of the program include sophisticated diagnostics of advanced fuels testing for nuclear reactors for the Department of Energy (DOE) Gen IV program, with the future capability to provide real-time measurement of strain in fuel rod cladding during operation *in situ* at any research or power reactor in the United States. By quantifying the stress and strain in fuel rods, it is possible to significantly improve fuel rod design, and consequently, to improve the performance and lifetime of the cladding. During the past year of this program, two sets of experiments were performed: small-scale tests to ensure the reliability of the gages, and reactor pulse experiments involving the most viable samples in the Annulated Core Research Reactor (ACRR), located onsite at Sandia.

The ACRR experiments were performed to support Sandia National Laboratories' active pursuit of an advanced fuels testing program to be operated in Tech Area III/V. As the United States moves forward in its attempt to build newer, more advanced nuclear reactors, next-generation fuels need to be fabricated and tested to ensure safety and keep proliferation risks to a minimum. To feasibly certify new types of nuclear fuel, highly developed diagnostics must be able to accurately measure the degradation of the testing material without being compromised itself , because the transient Verification and Validation (V&V) testing of the fuel will occur within a reactor environment.

Fuel cladding is the material that provides containment and protection for the encapsulated nuclear material. Fuel cladding fails as a result of the strain and stresses that occur in the fuel as it swells due to the fission gases produced during the life of the fuel. Sandia National Laboratories is a leader in the research to develop ways to perform strain measurements in this type of environment, where a transient magnetic field, extremely high temperatures, and high neutron fluxes greatly affect the traditional workings of a strain gage.

To determine the proper gages to use for future fuels-testing programs, trial experiments were constructed on site in Tech Area V, culminating in a larger-scale experiment in the ACRR, also located in Area V.

Research into strain gages began with off-the-shelf, commercial strain gages and adhesives to determine how strain was created in a cylindrical surface, as is the case with most types of fuel cladding. The small, tabletop experiments showed that cylindrical strain in a pipe is simple to measure accurately and could be adjusted for the influence of temperature at any point. The commercial gages were found to be extremely effective; however, the adhesive techniques available could not guarantee a sufficiently strong bond to deal with the elevated temperatures that would be seen in a traditional light-water reactor (LWR), approximately 500-600 °C.

2. THEORY AND ENGINEERING OF STRAIN GAGES

Stress is a natural phenomenon that occurs within any material. The force applied to a material is absorbed within a unit area of the material, causing stress in the object. The stress imparted on that object is directly related to the amount of strain. For example, if 100 pounds of force is applied directly onto a 1' by 1' piece of rubber, and 100 pounds is applied in the same fashion onto a 1' by 1' piece of stainless steel, each object experiences the same stress (force per area; See Eq. 3). However, the two materials react very differently to the applied force. The strain in each material is characterized by inherent material properties, such as Young's Modulus (E) and Poisson's Ratio (ν). These are utilized to determine the mode and degree of deformation (the amount of strain) that will occur when a material is exposed to a given stress (See Eq. 2 and Eq. 17).

Stress in an object cannot be directly measured, and must be derived from measured values through a strain gage, essentially a resistor with a specific nominal resistance. A strain gage is "adhered" in some fashion to the material substrate undergoing the strain. During operation, a voltage is applied across the strain gage, allowing current to flow. When a force is applied to the substrate, the changing cross-sectional area of the strain gage causes a change in resistance for the gage and alters the output voltage of the circuit. If the resistor is in the proper arrangement (a Wheatstone bridge, which will be discussed later), then the voltage signal read from a strain gage can be correlated to a true value of the strain. The signal readout per unit change in resistance is given by the particular strain gage's sensitivity, or "gage factor". (See Eq. 21.) This provides a natural "amplification" of the output voltage signal: a strain gage with larger gage sensitivity will produce a larger output voltage for the same strain on the substrate. However, this property is not always desirable, because a large sensitivity can amplify electrical noise, making it difficult to discern true strain values from within the experimental results.

2.1. Wheatstone Bridge

A Wheatstone bridge is a device used to measure loads and strains on an object. It is a circuit consisting of four resistors that provides an excitation voltage in the circuit based on changes in the values of the resistors. As a resistor in the bridge changes its resistance, it "unbalances" the circuit, the value of which is based upon the nominal resistances of three other resistors, or strain gages. This signal can be then be correlated to an actual value of load or strain. If measurements are not taken with four different resistors, then a (Wheatstone) bridge completion module must be present to allow meaningful data to be collected. The Wheatstone bridge setup, therefore, comes in three different types: Quarter, Half, and Full Bridge setups. Figure 1 depicts a full Wheatstone bridge.

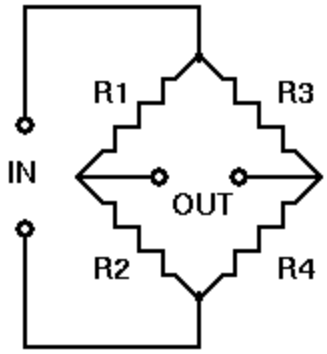

Figure 1. Wheatstone Bridge consisting of four resistors.
A single Wheatstone bridge can have up to four active gages. However, if fewer gages are utilized, the remaining "arms" of the bridge must be filled with a Bridge Completion Module (BCM) or external resistors.

A Quarter-Bridge I configuration involves only one active gage for measurement. This configuration does not allow for "temperature compensation" of the circuit, in which two adjacent "arms" of the Wheatstone bridge inherently subtract out common resistance changes. During early experiments, this quality was unnecessary, given that only pressure measurements at room temperature were desired. In the Wheatstone bridge, the "active" gage registers strain due to both temperature and mechanical stretching of the gage. Therefore, to temperature-compensate a strain measurement, a Quarter-Bridge II or Half-Bridge I configuration must be used.

The Quarter-Bridge II configuration involves a "dummy," or non-active, gage installed into the Wheatstone bridge. This dummy gage is attached to the substrate in such a way that the non-active gage is sufficiently close to the active gage, so that each gage measures the same value of strain due to temperature. However, the non-active gage is allowed to nearly "free-float" next to the pipe, being only tacked on by a corner of the gage. The difference in the two registered values for each strain gage provides a true value of strain due to pressure. All Quarter-Bridge configurations require a bridge completion module, which connects the remaining stable resistors necessary for the bridge.

For some applications, such as load bearing on a support beam, the half-bridge and full-bridge configurations should be used to measure strain. A half-bridge utilizes two active gages as part of the Wheatstone bridge. A Half-Bridge I uses one active gage and one "compensating" gage, where the two gages are aligned orthogonal to one another. Poisson's ratio is incorporated to the value of the second gage to attain an output voltage for the Wheatstone bridge. A Half-Bridge II configuration uses two active gages, with both gages measuring the same direction of strain, to double the output voltage of the circuit. Each of these Half-Bridge configurations still requires a bridge completion module to function properly. A full-bridge consists of four active gages; no bridge completion module is needed, because all four arms of the Wheatstone bridge consist of active gages. The four strain gages can be set up all in parallel, two parallel with two perpendicular, or other configurations. However, when installing a full Wheatstone bridge, it is important to align opposite sides of the bridge with the same alignment (parallel or perpendicular to principal strain direction) and the same nominal resistance. For example, R1=R2 and R3=R4,

as depicted in the typical arrangement of a Wheatstone bridge in Figure 1. The Quarter-Bridge I configuration was exclusively used in the experiments discussed in this report.

2.2. Utilization of Omega Strain Gages

This LDRD study aims to quantify the effects of strain due to pressure and temperature on a cylindrical pipe. The first step in the program was to complete preliminary, small-scale experiments onsite at Sandia National Laboratories to provide a benchmark for future strain gage tests. During all these "tabletop" experiments, ½-inch diameter SS316L tubing, having a wall thickness of 0.035 inches, was used.

When calculating strain in a cylindrical pipe, a distinction between thin- and thick-wall pressure vessels must be made. A vessel is defined as "thin-walled" if the ratio between the inner radius and the wall thickness is greater than 10. Therefore, the sample tubing used for the small-scale tests qualifies as "thick-walled." Using a free-body diagram, the stress can be calculated for both axial (longitudinal) and circumferential (hoop) directions of the pipe. (See Eq. 4 through Eq. 12.) For thin-wall vessels, the circumferential strain is twice the axial strain. See Figure 2 for clarification of axial and circumferential directions in a pipe.

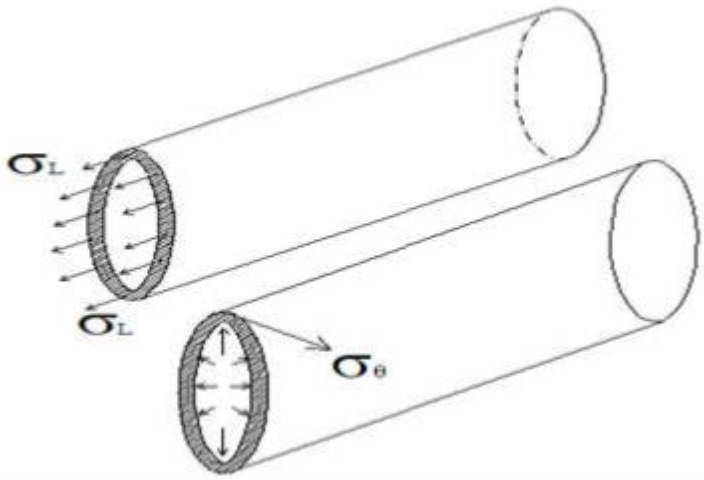

Figure 2. Axial and Circumferential Stress in a pipe.

A thick-wall pipe has an inner-radius-to-wall-thickness ratio smaller than 10. For the tabletop studies, the SS316L pipe qualifies as a thick-wall pressure vessel. (See Eq. 13 through Eq. 14.) The strain in a thick-wall pressure vessel is affected by the material of the vessel, the inner and outer radii of the cylinder, and the internal and external pressures acting on the vessel. Unlike thin-wall vessels, the stresses in the axial and circumferential directions in a thick-wall vessel do not differ by a simple factor of two. The difference depends on a material property called "Poisson's Ratio" (ν, see Eq. 18). Poisson's Ratio is the ratio between hoop strain and axial strain. To illustrate this property, assume that two equal, opposite forces are applied to a rubber cylinder along its axis. This causes the cylinder to stretch axially (lengthen). At the same time, the radius decreases, causing hoop stress to be accumulated (hoop compression in this scenario), though only axial force is applied. Poisson's ratio is used to quantify this relationship. If the force is applied only from the inside, such as a pressurized pipe, the axial strain can be modeled

simply as a function of the hoop stress (See Eq. 17). Furthermore, if the pipe is exposed to temperature changes, then an additional term ($\alpha\Delta T$) is included to the value of strain due to pressure to attain a total strain value (See Eq. 15 and Eq. 16), where α is the thermal coefficient of expansion of the strain gage and ΔT is the difference between the current and initial temperatures of the material. The value of α should be approximately equal to α of the substrate to avoid thermal separation between the gage and the substrate. The tabletop tests experimentally confirmed the necessity to include the additional term in strain calculations.

For the tabletop experiments, only the KFG series of strain gages from Omega were used. Readily available and inexpensive, these gages were used in exclusively Quarter Bridge I configurations. The Omega KFG strain gage is a foil resistor strain gage, available in a variety of nominal gage resistances and physical sizes. Table 1 lists the types of strain gages from Omega that were used in the tabletop tests.

Table 1. Omega KFG-series Strain Gage varieties utilized during preliminary tests at Sandia National Laboratories

Number of Wires	Nominal Gage Resistances (Ω)	Length (mm)
2-wire	120	2, 10
	350	3
3-wire	120	2, 10
	350	3

The gages purchased from Omega consisted of gages 2 mm, 3 mm, and 10 mm long, and having a resistance of either 120 or 350 ohms. All 2 mm and 10 mm gages had a nominal gage resistance of 120 ohms; all 3 mm gages had a nominal resistance of 350 ohms. Within this assortment, the Omega KFG series is available in two more varieties: 2-wire and 3-wire.

The 2-wire is the simplest version of a strain gage. Introducing a third wire compensates for any lead-wire resistance that occurs as a consequence of long instrumentation lead wires, which can alter the nominal resistance value of a single arm of the Wheatstone bridge, thereby producing inaccurate strain results. The third wire shares a strain gage solder terminal with a second wire, because a thin foil resistor only has two connections. In a two wire-gage, the second terminal must be jumped (with ideally zero resistance) to create a third terminal at the point of the bridge completion module, because three terminals are required for a completed Wheatstone bridge in Quarter I configuration. A third wire eliminates the need for a jumped wire, allowing current in the gage to be split among the second and third terminals, instead of exclusively to the second terminal in the bridge completion module. Obviously, for this to be accurate, all three of the lead wires attached to the strain gages must be the same length.

A list of their properties is included with purchased strain gages, including a chart depicting how the gage factor, a property of the strain gage (See Eq. 21) changes with increasing temperature. For calculations performed in this experiment, this option was ignored due to its negligible influence on the results.

During installation, it was observed that 120 ohm gages were more susceptible than 350 ohm gages to slight signal drifts (delta R/R), but it was also observed that 120 ohm gages performed better if the 10 mm gage was aligned circumferentially and the 2 mm gage was aligned axially, to take advantage of and avoid curvature, respectively. The 120 ohm gages are more sensitive because a smaller change in resistance (force applied) leads to a larger output voltage.

Therefore, 120 ohm gages are better for small measurements, but are undesirable, due to their inherent sensitivity, if a large amount of electrical noise is anticipated during experiments. Gages of 350 ohm are less sensitive to applied forces, but also can be affected less by extraneous noise.

2.3. Installation of Omega Strain Gages

The Omega KFG-series foil-type strain gages were the only type installed for the tabletop tests; this section will not consider other strain gage types.

A successful bond for a strain gage requires a clean surface of the substrate as a work space. Manufacturer recommendations for installation of the Omega KFG strain gages require that surface preparation include, but not be limited to: grit blasting, dry rough sanding, dry fine sanding, wet fine sanding, and a two-step solvent cleaning of the substrate. Based on the long-term goals of this LDRD, a minimal amount of surface preparation is desired due to abrasion and temperature restrictions for future fuel cladding samples. As a result, the only cleaning mechanism used for these experiments was ethanol or acetone wipes to clear the substrate of fine particles and possible oxidation layers. It should be noted that this does not fully satisfy the recommendations from Omega.

Installation of these gages should be practiced to better produce useable samples. Being able to repeat the successful installation of the gages is essential. The following procedure was used for all Omega KFG-series strain gage installations for the tabletop tests:

- Once the surface of the substrate is cleaned with either ethanol or acetone, alignment marks are needed to properly position the strain gage, either axially or circumferentially:
  - Each direction requires a separate alignment technique.
  - It is important to note that these techniques are not precise. All are done in a tabletop/laboratory environment and are judged by hand-eye coordination.
  - Also, an error in angular precision when installing a gage to measure strain is least important when aligning the strain gage in the axial or circumferential directions, as shown in Eq. 19 and Eq. 20.
- For circumferential alignment, a curveable straight edge (the side of a sheet of 8.5-inch x 11-inch paper) was bent around the ½-inch pipe several times. Each sequential edge was lined up and marked with a fine tip sharpie, producing a straight line in the circumferential direction.
- For axial alignment, a 1/8-inch diameter SS316L pipe was used. The 1/8-inch tube was held on top of the ½-inch pipe so that it created a level at the interface of the two. The interface is marked to create a straight line on a cylinder in the axial direction.
- Once surface preparation and alignment marks are made, it is time to prepare the gage.

    - The strain gage should never be touched with the experimenter's bare hands due to potential contamination from oils present in human skin, which would affect the delicate adhesion process.
- Gently lay the strain gage on top of a petri dish, or another kind of smooth, plastic surface. The strain gage should be right side up, with the mounting side of the strain gage on the bottom.
- Using Teflon film tape, cover the strain gage completely, taping so that no air bubbles are formed between the tape and the petri dish or the tape and the strain gage.
    - It may be handy to create tabs on the ends for the Teflon tape for easily handling.
- Remove the tape AND the strain gage in one pull, removing the tape at an obtuse angle so that the strain gage remains fairly flat during removal.
- Align the gage using the marks on the strain gage and the marks created by the installer on the pipe.
- Tape the strain gage down into position on the pipe.
- Lift the tape and strain gage at an obtuse angle, just enough so that the entire strain gage is lifted off the pipe while leaving the Teflon tape attached to the pipe, keeping the previous alignment.
- Apply a small amount of the desired adhesive just BELOW the strain gage, where the Teflon tape has been applied.
- Moving along the strain gage, apply a very thin layer of glue to the bottom portion of the strain gage.
- In one swift motion, replace the strain gage smoothly on the pipe, attempting to create an even coat of adhesive to bond the strain gage to the SS316L pipe.
    - At this point, the installer should be pressing his or her fingers down on top of the Teflon tape directly above the strain gage, since the glue is heat-activated by body temperature.
- Hold on top of the strain gage, continuous changing pressure points on the strain gage for a full minute. At this point, the glue is bonded, but will take approximately another 24 hours to completely cure. (The glue is discussed later in this section.)
- On the next day, the glue should appear dried. If the adhesive still appears to be a liquid, then it is NOT cured.
- Using the tabs you created the previous day on the Teflon tape, lift at a sharp angle to remove the tape while leaving the strain gage bonded to the pipe.
    - When removing the tape, make sure that it is the alternate corners that are being lifted up, instead of two adjacent corners at the same time.
- The recommended approach is to remove the corners lacking solder pads first to avoid undue stress on the solder pads or wires. Figure 3 shows a completed sample.

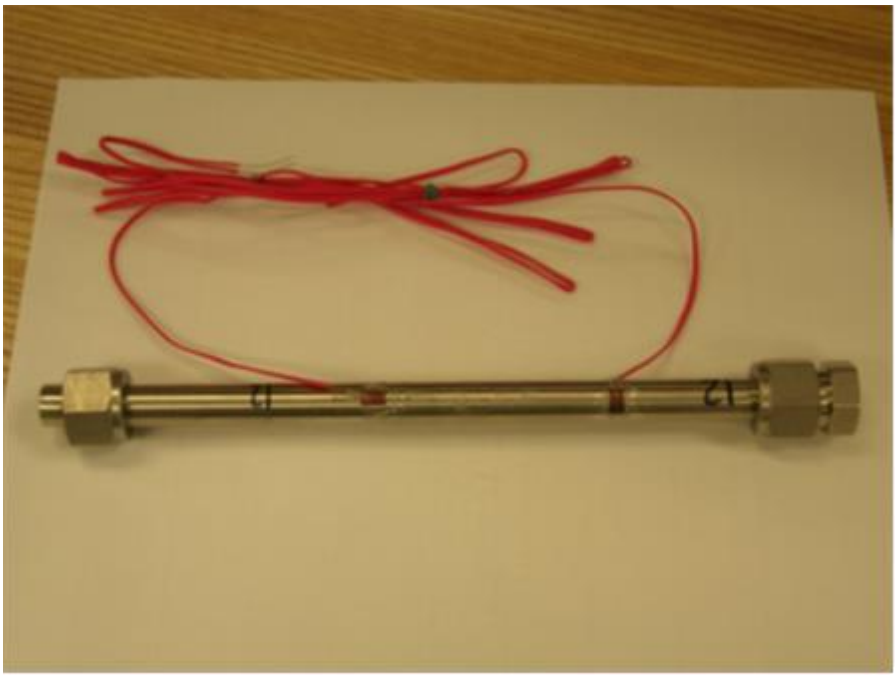

Figure 3. A completed strain gage sample mounted on a 1/2" SS316 pipe. Pictured is a 2-wire, 3 mm, 350 ohm gage from the Omega KFG-series.

To effectively measure strain, the strain gage should stretch the same amount as the substrate to which it is attached, so proper adhesion is essential to a good strain measurement. In this case, the substrate will be the SS316L pipe. The adhesive used in all of these experiments is methyl cyanoacrylate (SG 496, for use with metals) or ethyl cyanoacrylate (SG 401, for use with organic materials), two kinds of widely-used quick-drying glue, both purchased from Omega. Both were utilized, and there was little observed difference between the two adhesives. See Appendix B for more information about strain gage installation.

2.4. Calibration for Omega Strain Gages

A "shunt calibration" is designed to calibrate a voltage signal produced by a measurement device (i.e., a strain gage) to a real world value, in this case strain (ultimately for units of microstrain, or μin/in).

There are two ways to accomplish this. For the tabletop experiments with the Omega KFG gages, two types were used: a manual calibration and an automated process. Purchased from Omega, a BCM-1 (Bridge Completion Module-1) was used to complete the Quarter I Wheatstone Bridge, and DP41-S Shunt Calibration units were used for this portion of the experiment. The strain gage was connected to the BCM-1, and the BCM-1, in turn, was connected to the Shunt Calibration unit. The DP41-S simply puts out a numerical signal, corresponding to the voltage it receives as an input (usually in millivolts). Figure 4 displays an image of the DP41-S and the BCM-1.

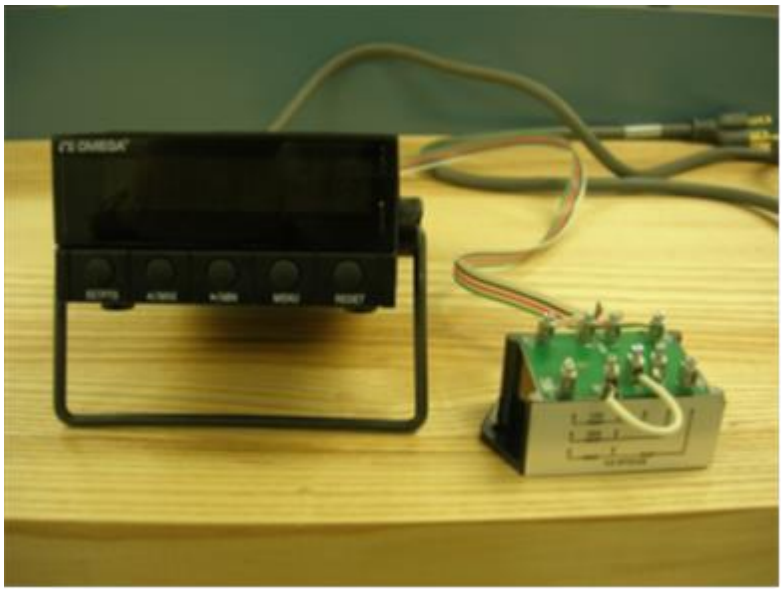

Figure 4. DP-41S Shunt Calibrator (left) and BCM-1 (right) used for tabletop tests. BCM-1 has circuit for both 120 and 350 ohms.

Once connected to the system, the DP41-S is zeroed while no strain is present on the gage. Then, using a potentiometer, an artificial resistance is connected in parallel with the active strain gage. The value of the potentiometer is specified based on both the nominal resistance and the gage factor, according to a table in the Strain Gage User's Handbook (See Figure 5).

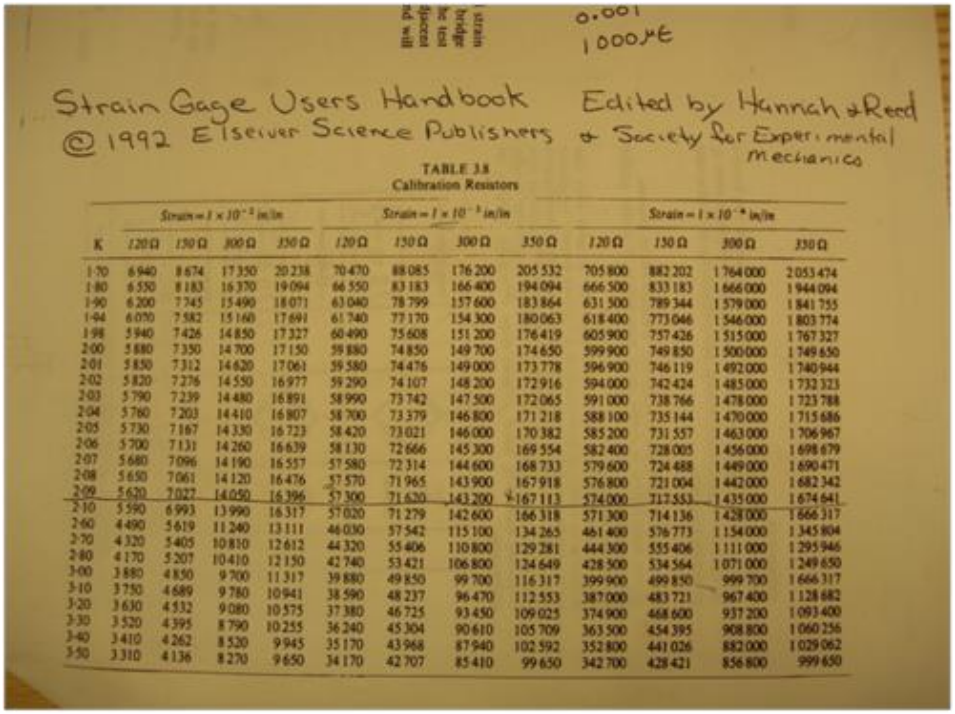

0.001
1000με

Strain Gage Users Handbook
© 1992 Elsevier Science Publishers

Edited by Hannah & Reed
& Society for Experimental Mechanics

TABLE 38
Calibration Resistors

	Strain = 1 × 10⁻² in/in				Strain = 1 × 10⁻³ in/in				Strain = 1 × 10⁻⁴ in/in			
K	120 Ω	150 Ω	300 Ω	350 Ω	120 Ω	150 Ω	300 Ω	350 Ω	120 Ω	150 Ω	300 Ω	350 Ω
1·70	6 940	8 674	17 350	20 238	70 470	88 085	176 200	205 532	705 800	882 202	1 764 000	2 053 474
1·80	6 550	8 183	16 370	19 094	66 550	83 183	166 400	194 094	666 500	833 183	1 666 000	1 944 094
1·90	6 200	7 745	15 490	18 071	63 040	78 799	157 600	183 864	631 500	789 344	1 579 000	1 841 755
1·94	6 070	7 582	15 160	17 691	61 740	77 170	154 300	180 063	618 400	773 046	1 546 000	1 803 774
1·98	5 940	7 426	14 850	17 327	60 490	75 608	151 200	176 419	605 900	757 426	1 515 000	1 767 327
2·00	5 880	7 350	14 700	17 150	59 880	74 850	149 700	174 650	599 900	749 850	1 500 000	1 749 650
2·01	5 850	7 312	14 620	17 061	59 580	74 476	149 000	173 778	596 900	746 119	1 492 000	1 740 944
2·02	5 820	7 276	14 550	16 977	59 290	74 107	148 200	172 916	594 000	742 424	1 485 000	1 732 323
2·03	5 790	7 239	14 480	16 891	58 990	73 742	147 500	172 065	591 000	738 766	1 478 000	1 723 788
2·04	5 760	7 203	14 410	16 807	58 700	73 379	146 800	171 218	588 100	735 144	1 470 000	1 715 686
2·05	5 730	7 167	14 330	16 723	58 420	73 021	146 000	170 382	585 200	731 557	1 463 000	1 706 967
2·06	5 700	7 131	14 260	16 639	58 130	72 666	145 300	169 554	582 400	728 005	1 456 000	1 698 679
2·07	5 680	7 096	14 190	16 557	57 580	72 314	144 600	168 733	579 600	724 488	1 449 000	1 690 471
2·08	5 650	7 061	14 120	16 476	57 570	71 965	143 900	167 918	576 800	721 004	1 442 000	1 682 342
2·09	5 620	7 027	14 050	16 396	57 300	71 620	143 200	167 113	574 000	717 553	1 435 000	1 674 641
2·10	5 590	6 993	13 990	16 317	57 020	71 279	142 600	166 318	571 300	714 136	1 428 000	1 666 317
2·60	4 490	5 619	11 240	13 111	46 030	57 542	115 100	134 265	461 400	576 773	1 154 000	1 345 804
2·70	4 320	5 405	10 810	12 612	44 320	55 406	110 800	129 281	444 300	555 406	1 111 000	1 295 946
2·80	4 170	5 207	10 410	12 150	42 740	53 421	106 800	124 649	428 500	534 564	1 071 000	1 249 650
3·00	3 880	4 850	9 700	11 317	39 880	49 850	99 700	116 317	399 900	499 850	999 700	1 666 317
3·10	3 750	4 689	9 780	10 941	38 590	48 237	96 470	112 553	387 000	483 721	967 400	1 128 682
3·20	3 630	4 532	9 080	10 575	37 380	46 725	93 450	109 025	374 900	468 600	937 200	1 093 400
3·30	3 520	4 395	8 790	10 255	36 240	45 304	90 610	105 709	363 500	454 395	908 800	1 060 256
3·40	3 410	4 262	8 520	9 945	35 170	43 968	87 940	102 592	352 800	441 026	882 000	1 029 062
3·50	3 310	4 136	8 270	9 650	34 170	42 707	85 410	99 650	342 700	428 421	856 800	999 650

Figure 5. A page from the Strain Gage User's Handbook, giving the resistances needed to artificially simulate strain in a Wheatstone bridge with one active gage.

The resistance suggested by the Strain Gage User's Handbook[1] in Figure 5 specifies the resistor value that would simulate one millistrain. This causes an "unbalance" in the Wheatstone bridge and creates an output voltage, because the potentiometer in parallel with the active gage is equivalent to a different resistance than the active gage alone. The DP41-S output therefore corresponds to one millistrain (it was adjusted three decimal places to record microstrain). When internal pressure is applied to the pipes, a value appears on the DP41-S, which can be related to the measured value of microstrain by the initial shunt calibration. This process worked fairly well for the initial experiments.

Automation was the next step for experimental shunt calibration of the strain gages. Instead of calculating every desired data point, experimental software from National Instruments (NI), called "Labview", can record data from the strain gages. However, the strain gage cannot simply be directly wired into any input module . An NI-9949 Quarter Bridge completion module must be used to allow the signal from the strain gages to be read into an NI-9237 module, which then communicates directly with Labview. The NI-9237 contains an internal 100 kΩ resistor, and can create an excitation voltage up to 10 volts (5 volts was used in all experiments) to flow the needed current through the Wheatstone bridge. Therefore, no manual shunt calibration is needed. Labview executes shunt calibration virtual instrument (VI) before recording data, allowing values to be recorded directly in microstrain, rather than output voltage.

2.5. Experiments

2.5.1. Laboratory Experiments in 6585/1408

The first set of tabletop experiments was performed shortly after installing the first strain gages. Recall in section 1.3 that some preparation steps were eliminated for future purposes. Therefore, it was unclear whether a cursory cleaning of the surface would be satisfactory to measure strain. A basic aluminum test stand was created to isolate the strain gage from any other sources of stress. The strain gage was wired into the DP41-S shunt calibrator, as discussed earlier. If strain was induced, the reading would change. A check of the installation was conducted, essentially to ensure that the strain gage registered any values at all, without a regard for accuracy. Force was applied to the end of the pipe and the voltage reading on the unit changed substantially. When a larger force was applied, the reading increased even more, as expected.

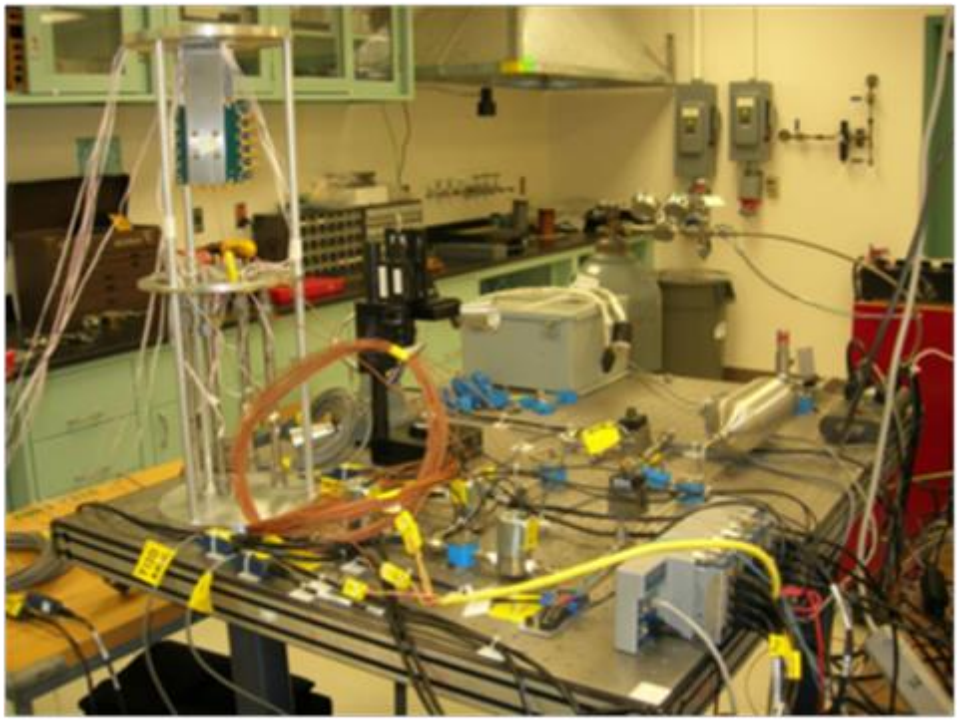

Figure 6. Tabletop experimental set-up used for small-scale tests of strain gages. Also pictured is the ACRR test stand used in later experiments.

The tabletop apparatus in Figure 6 was built to accompany the HiTec Products, Inc. (HPI) strain gages purchased in late spring 2011. The HPI strain gages failed in their preliminary evaluation due to incorrect fabrication, though the source of error is unclear. The HPI gages were constructed using a Rokide flame-spray technique; future methods for installing strain gages at Sandia using this technique will be discussed in later sections of this report. A scanning electron microscope (SEM) analysis done by Sandia researchers also indicated substantial structural errors in the HPI installation of the strain gage by Rokide flame-spray.

Though the HPI gages failed, the pressure system constructed for them was useful for testing the Omega KFG series strain gages, as discussed previously. The Omega experiments were done to measure the axial and circumferential strain on the pipe (See Eq. 15 and Eq. 16). The initial set of pressure tests were increased in increments of 100 psi, ramping from 100 psi up to 800 psi. This allowed for comparisons between predicted and measured values for strain due solely to pressure. A manual reading from the DP41-S shunt calibrator was used to gather data during the experiment. The hoop strain matched the predicted values well when compared, though axial strain did not. After several iterations of the pressure tests, the inaccuracy of the axial strain results never changed. Based on experimental evidence, it was concluded that a lack of axial stress in the pipe allowed Eq. 15 to behave like Eq. 17. Recalculating strain with the experimental data showed that Eq. 17 did accurately describe the behavior of the strain gages mounted axially. In addition, the ratio between the hoop strain and the axial strain was nearly the same in all experimental iterations, in accordance with Eq. 16.

The next set of data was collected following the installation of the NI 9237 modules. Recall that shunt calibration is performed completely internally and independent of the experimenter in the NI Labview software. Using both built-in and user-created VIs in Labview, strain data was recorded directly to the laboratory computer. Output values of strain matched experimental results very well. However, on initial set-up, the strain gage signal drifts in the value of strain, independent of temperature, pressure, or motion, as displayed in Figure 7. It can be concluded that this is an inherent property to the strain gage. The gage heats up, as all resistors do, so its gage sensitivity changes slightly as it reaches the steady-state condition associated with the 5V excitation voltage that the NI 9237 applies to each gage.

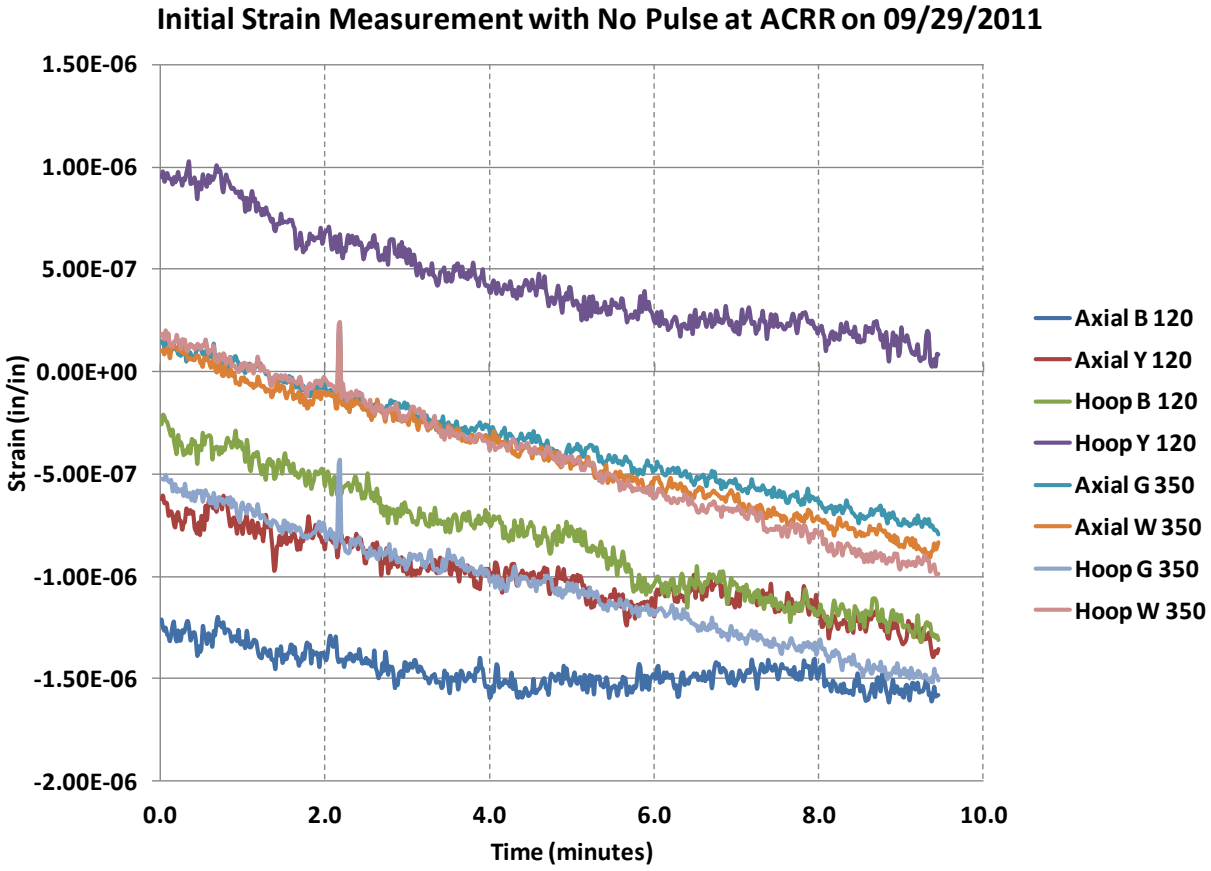

Figure 7. Initial Strain Measurements with No Pulse at ACRR on 09/29/2011. This figure demonstrates the initial "drift" of strain gages.

When an internal temperature is applied, each of the four strain gages showed approximately the same amount of strain (Eq. 15 and Eq. 16), which is predicted when the experiment does not include pressure. The coefficient of thermal expansion, α, is directly correlated to the strength of the bond between the strain gage and the associated SS316L pipe. By evaluating tabletop results for temperature, the value of α can be attained for the strain gage. Theoretically, this value should match α for the material of the substrate. Comparing the two coefficients indicates that the bond between the substrate and the gage is successful, despite the lack of efficient and sophisticated cleaning at the beginning of the sample fabrication.

Initial tests show that the strain gage was measuring strain in the pipe; however, it was unclear how accurate this strain measurement would be with an internal pressure.

2.5.2. ACRR Experiments Performed 09/29/2011

Further sets of tests were performed with the ACRR Test Stand apparatus, seen in Figure 8.

Figure 8. Test Stand apparatus used during the ACRR experiments. Four pipes are visible, each with two strain gages. The bundled wiring at the top of the assembly was needed for data acquisition during the pulses.

The decision was made to design a test stand with the potential to position eight strain gages adhered to four SS316L pipes (two gages per pipe), using varying strain gage types to fully investigate the inherent strengths and weaknesses, as described earlier.

Commercial strain gages and commercial adhesives were used to fabricate the four samples. These samples were lowered into the ACRR and subjected to five “pulses” of increasing energies. A pulse is a phenomenon only available in a research nuclear reactor, which creates a large amount of energy that is released in a very short amount of time. Because of this, long-term effects can be determined for samples without needing to experiment for long periods of time, allowing the results from our samples to be accurate in showing how the strain gages would react in a nuclear reactor over extended periods of use.

The experiment confirmed that the Omega KFG-series strain gages were sufficiently strong to withstand the temperature and neutron flux from the reactor. The results also indicated (as

suspected) that the adhesives used are not strong enough to withstand the high temperatures or neutron fluxes that exist in a hostile environment, such as the nuclear reactor. Therefore, the majority of future resources for the fuel testing diagnostics are being focused on research into these areas, such as advanced adhesive materials or flame spray installation.

Interestingly, the magnetic field created in the nuclear environment was compensated for in the experimental design by utilizing coaxial cables within a metal sheath, which dissipated potential eddy currents in the wires connecting the strain gages (they are essentially resistors) to the instrumentation and data acquisition systems.

The tests in the ACRR provided excellent results, allowing the fuels testing program to continue forward in its current state of development. The ACRR is capable of many pulses each day, with a variety of adjustable characteristics available for fine-tuning each individual pulse. Therefore, as advanced diagnostics, such as strain gages, are developed, they will continue to be tested exclusively on site.

Figure 9 through Figure 12 display the results from each experiment.

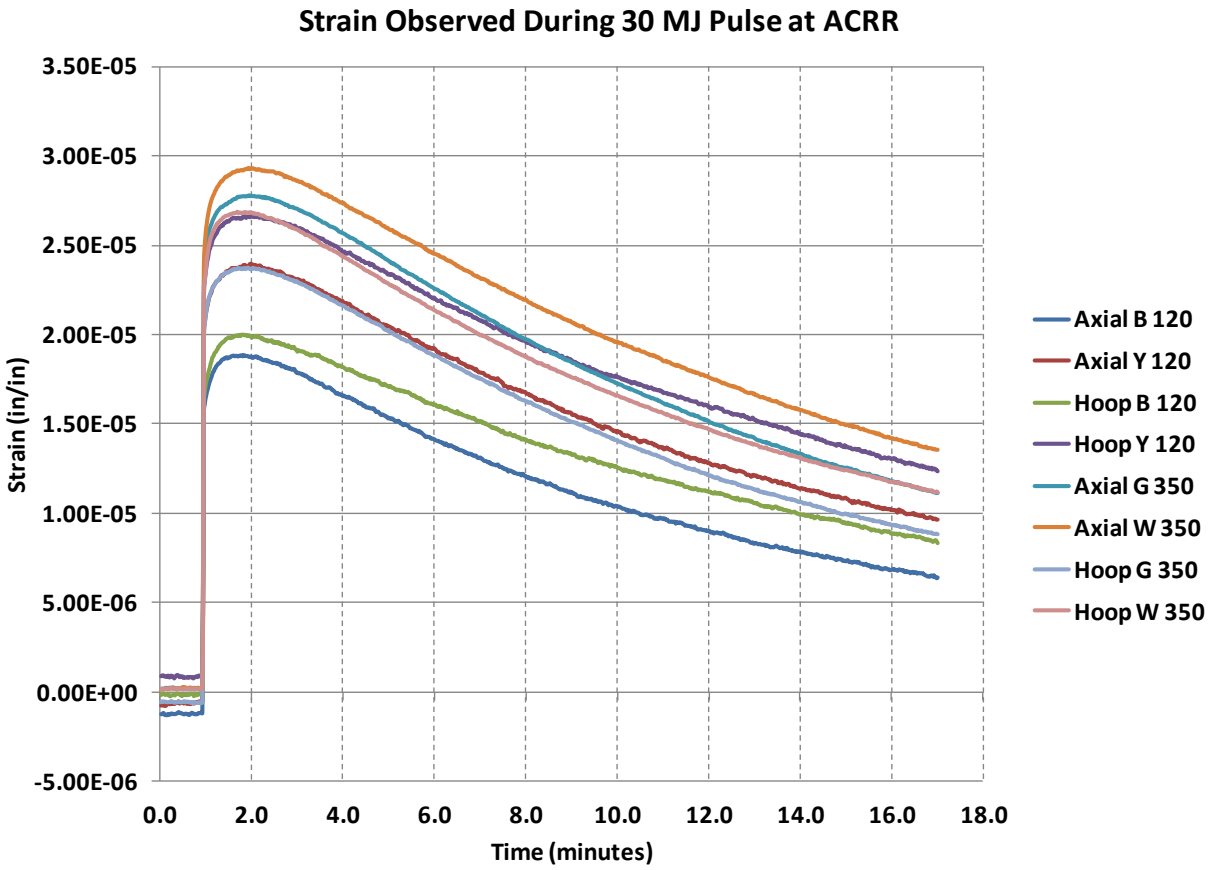

Figure 9. Strain Observed During 30 MJ Pulse at ACRR on 09/29/2011

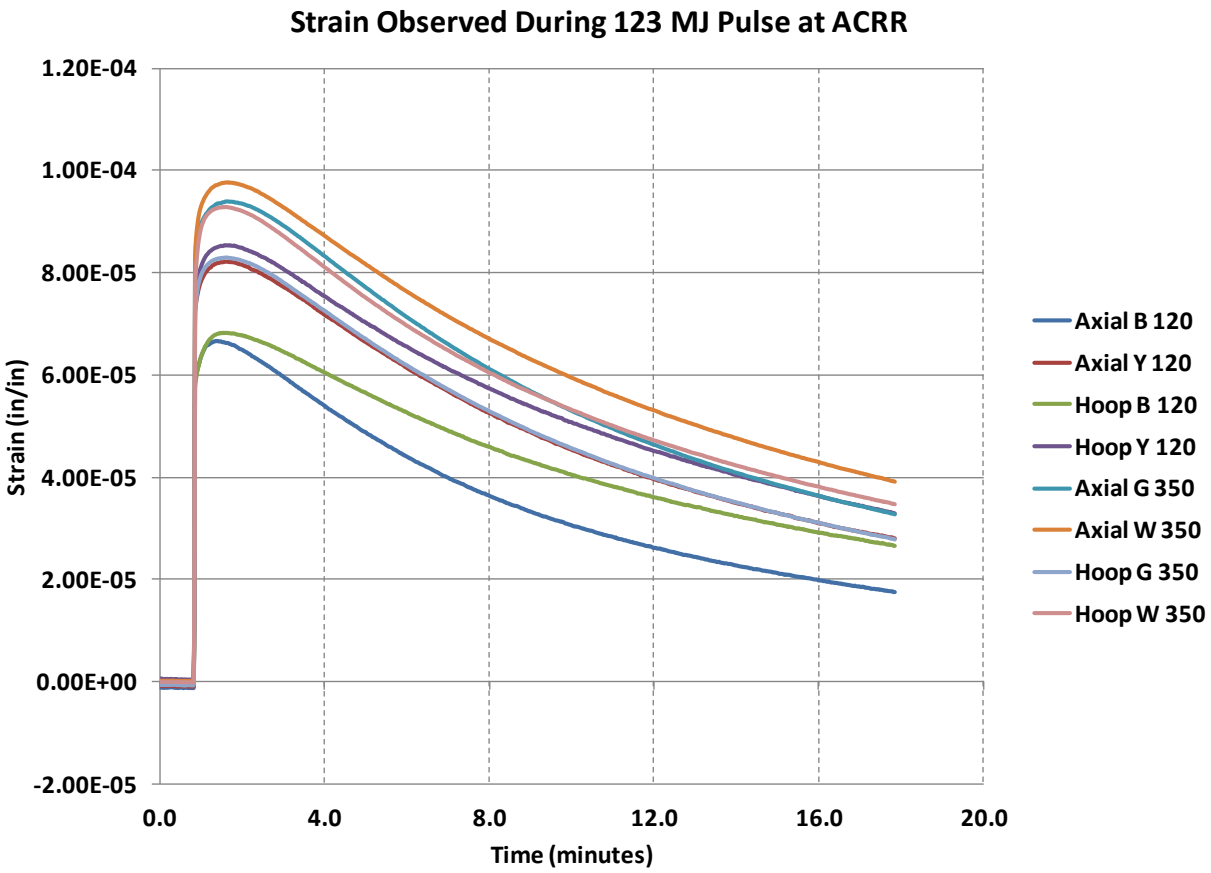

Figure 10. Strain Observed During 123 MJ Pulse at ACRR on 09/29/2011

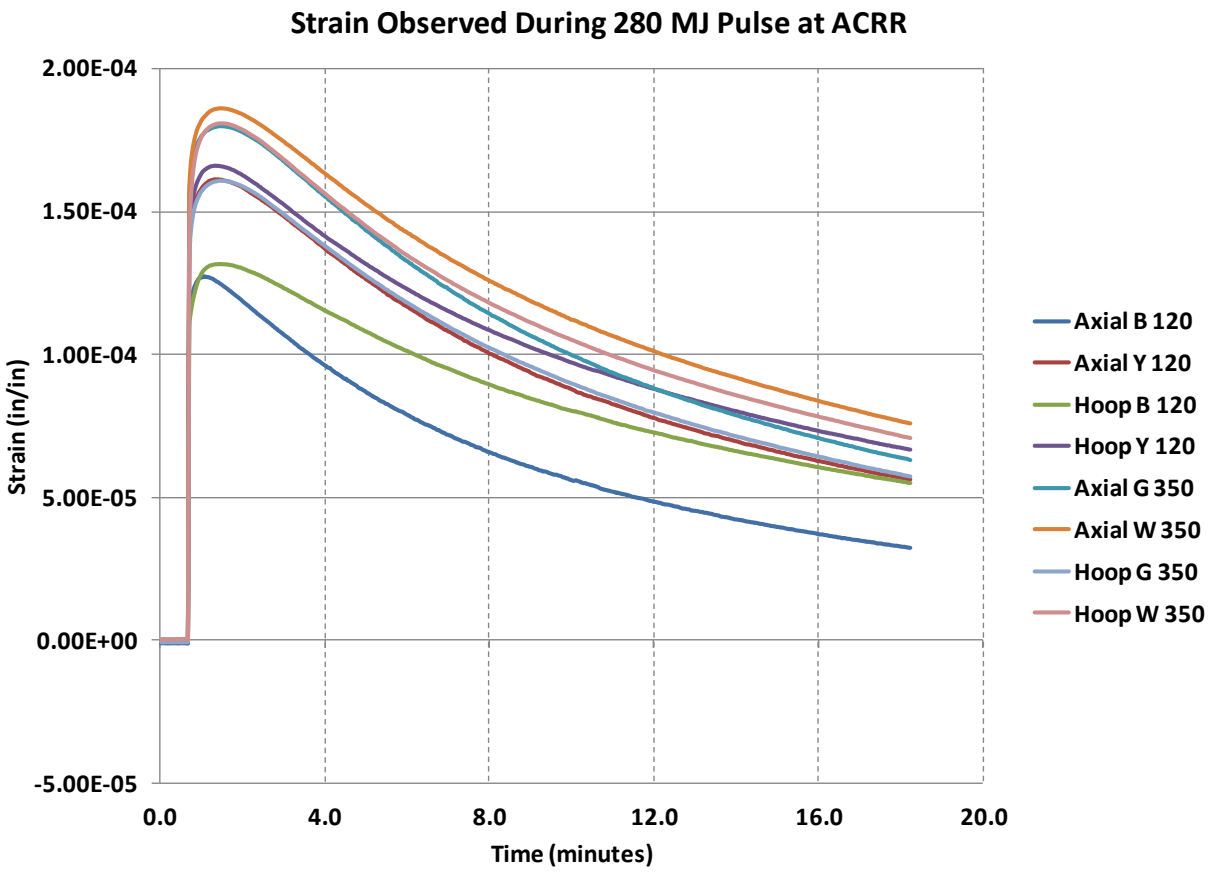

Figure 11. Strain Observed During 280 MJ Pulse at ACRR on 09/29/2011

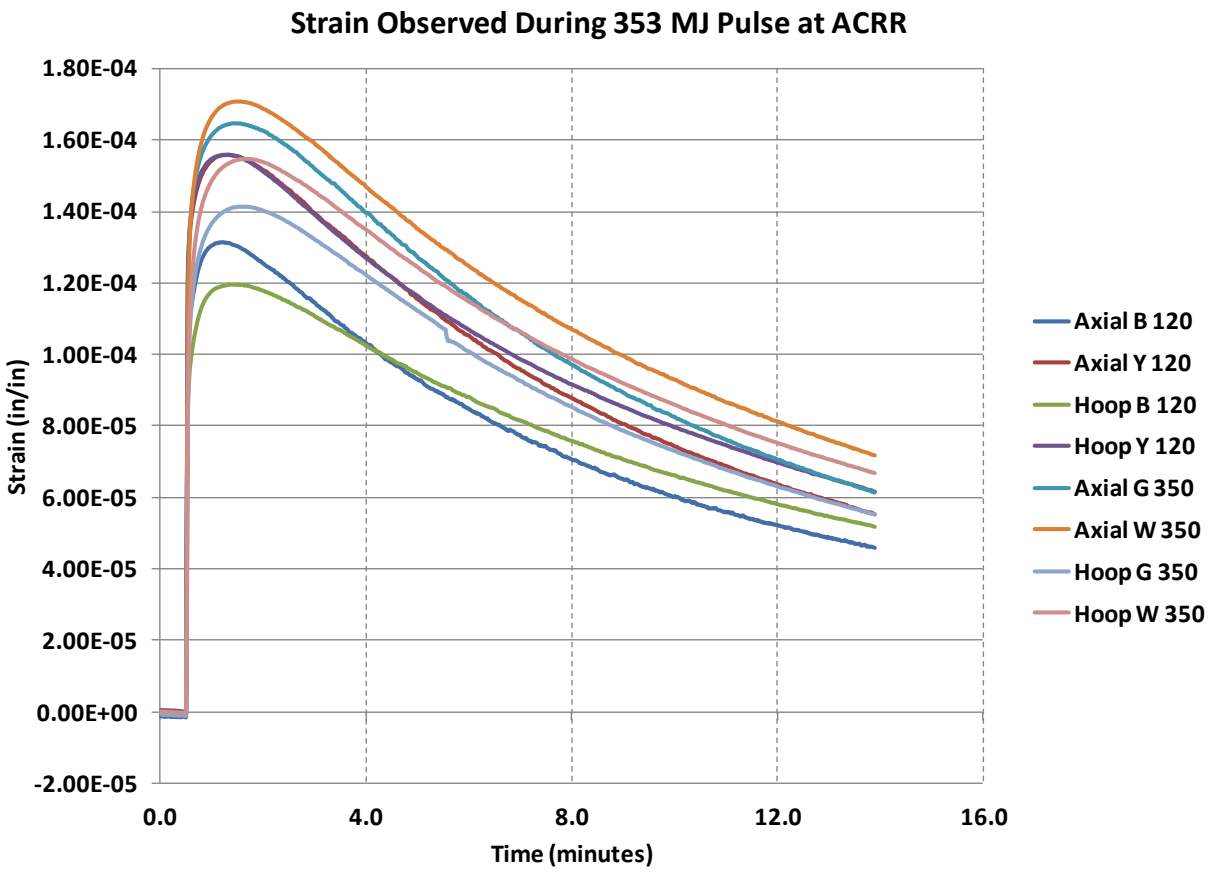

Figure 12. Strain Observed During 353 MJ Pulse at ACRR on 09/29/2011

The gages appear to respond predictably to temperature. A sharp spike upwards during the pulse is followed by a slow decay back to equilibrium temperature. The strain exhibited in the figures is only due to temperature, since the samples did not contain pressurized gas.

In all four viable tests, the strain gages have different values of strain, but appear to be essentially the same order of magnitude of strain. This would suggest that either: a) the nulling function in the Labview program could not successfully zero the strain value for all the strain gages due to existing interference or noise from the reactor environment, or b) the neutron flux was not uniform throughout the volume containing the samples, causing each strain gage to receive a different neutron flux and local temperature.

Based on the fact that there was very little noise in the actual signal, especially during pulse decay, which contains the largest amount of electromagnetic interference, option b) from above most likely indicates the true phenomenon observed during the shots. Also, there are only small differences in strain (on the order of 5 microstrain) between similarly aligned gages, which also supports the observations from option b).

It is interesting to note how little noise in the strain signal was observed. This is due to either negligible interference from the EM and neutron sources in ACRR or that precautions taken with the cable shields successfully prevented signal interference.

Finally, the 353 MJ pulse (the last case) indicates an improper signal from all the strain gages. For each pulse, a ratio was calculated between the measured strain of the highest value for strain (Axial W 350) and the predicted strain due to temperature. This value, due to differences in coefficient of thermal expansion differences of the steel and strain gage, should be approximately 3. This holds true until the 353 MJ pulse, where this value jumps to almost 6. The 353 MJ pulse actually indicates a decrease in strain from the 280 MJ pulse values. Therefore, the 353 MJ pulse was sufficient to separate the backing or the glue from the surface of the SS316L piping. Due to the uniform installation for all eight strain gages, the error due to this substrate ablation is roughly the same. By observing the graphs for the 280 MJ and 353 MJ pulses, it can be seen how much the strain in the 353 MJ pulse differs from a sensible value.

3. RADIATION EFFECTS ON STRAIN GAGE SYSTEMS

Radiation damages a strain gage signal in two distinct manners: electrical interference or structural degradation of the strain gage

During normal operations in a nuclear reactor, a steady electromagnetic field is present. The strength or direction of the field does not change with time; therefore, it does not significantly affect any electronic diagnostic equipment that may be present within the reactor vessel. However, in an experimental nuclear reactor, such as the ACRR, located onsite at Sandia National Laboratories, reactor pulses are used to substantially increase reactor power for a short amount of time. This transient event can cause the steady electromagnetic field to alter its magnitude and direction, though this does not cause excessive signal fluctuation from the strain gage to the above-ground instrumentation. In fact, it can be shown that a typical reactor produces current increases of 0.065 A per meter of cable for a 7,000 kW power change for the reactor.

In addition, electromagnetic waves travel at the speed of light. Any difference on the strain gage signal output influenced by the electromagnetic wave will occur extremely quickly, with the effects decaying quickly away in the signal from the strain gages to the instrumentation. During pulses at the ACRR, signal inputs from the strain gages were averaged every 10 signals, sampled at 10 Hz. This enables the user to decrease signal sensitivity, creating an experimental data point every second. Therefore, it is unlikely that any electromagnetic interference could effectively alter the voltage signal or even be measured.

3.1. Structural Degradation of the Strain Gage

The resistive, Omega KFG-series foil-type strain gages used in the ACRR experiments are characterized by three main components: etched constantan, a copper-nickel alloy, a polyimide backing, and nichrome lead wires.

In a nuclear reactor, material degradation can occur when exposed to a high neutron flux. The neutrons affect the strain gages by “interacting” with the atoms in the gage components. However, not all atoms interact with neutrons at the same rate. In fact, some elements (boron, cadmium) have extremely high interaction “cross sections,” and absorb neutrons readily. When

absorbed, the extra neutron can cause the atom to become unstable and may lead to radioactive decay that alters the atomic composition of the material. For example, if an aluminum atom absorbs a neutron, it becomes unstable, ultimately releasing a beta particle and leaving the original atom as the element silicon.

If the original aluminum was in a structural material, such as a plate or beam, then the material characteristics (Modulus of Elasticity, Poisson's ratio, etc.) may be altered. This can lead to material failure. Overall, this is the most important aspect of material degradation that would be expected in a strain gage. The degree of the material degradation depends on the overall "interaction" rate between the strain gage components and the neutron population of the reactor.

Constantan is a copper-nickel alloy and is the material basis for the strain gage "foil" itself. Constantan has constant material properties over a wide range of temperatures, making it ideal for high-temperature strain gage applications. Its constituents, copper and nickel, have mid-level neutron interaction properties, allowing a large neutron flux to potentially negatively influence the material integrity.

The polyimide backing is an organic material consisting entirely of carbon, nitrogen, and oxygen. These elements have extremely low neutron interaction rates, so material degradation is not expected in the strain gage foil backing at any neutron flux.

The strain gage lead wires are made of nichrome, a lead, copper, and nickel alloy. Nichrome has neutron interaction characteristics similar to that of constantan.

Therefore, based on the material composition of the strain gage components, it is most likely that if any material degradation occurs, it will be in the strain gage foil grid or the lead wires.

4. BEYOND RESISTIVE STRAIN GAGES

The progression of strain gage technology applicable in this area leads to gages that require flame-spray installation. To informally "certify" the Rokide-applied gages, a suitable porosity/application technique needs to be determined. The three parameters to consider are temperature of the spray, porosity of the Rokide layer once it dries, and modulus of elasticity (Young's Modulus) for the sprayed-on layers. The modulus of elasticity of the alumina depends greatly on the first two characteristics. Also, the coefficient of thermal expansion (α) of the layers should be greater than that of substrate (SS316: 16.5e-6 in/in°C), so that the layers don't "resist" the strain gage as it expands. Based on the HPI sample, a proprietary Sandia design can define characteristics for porosity of the layers with the constraint of maximum temperature for the cladding during plasma spray installation. A successful test matrix for this research should include an even distribution of axial and circumferential gages to experimentally determine the effect of curvature for the layers. An ideal Rokide flame-sprayed gage is shown in Figure 13.

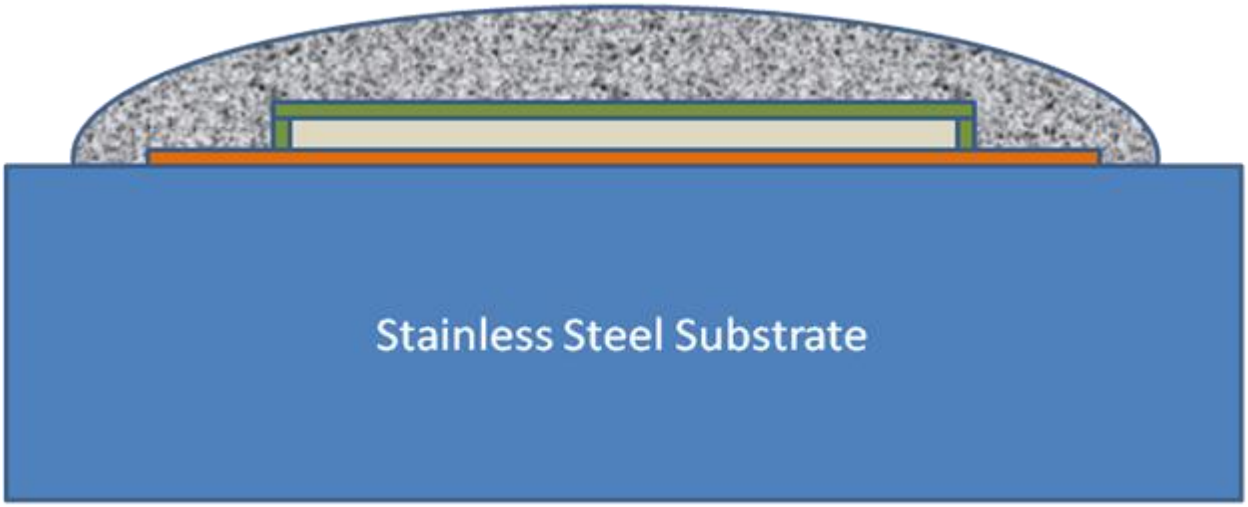

Figure 13. Ideal construction of a Rokide Flame-spray High Temperature gage. The gage is represented by the gray rectangle, while various layers of alumina flame-spray are displayed as the remaining shapes.

Rokide installation requires that a layer of Ni-Al_2O_3 is applied in order to create a smooth transition of properties from the SS to the Al_2O_3, which is the second layer of the installation. Rokide installation will utilize special gages from Vishay, shown in Figure 14.

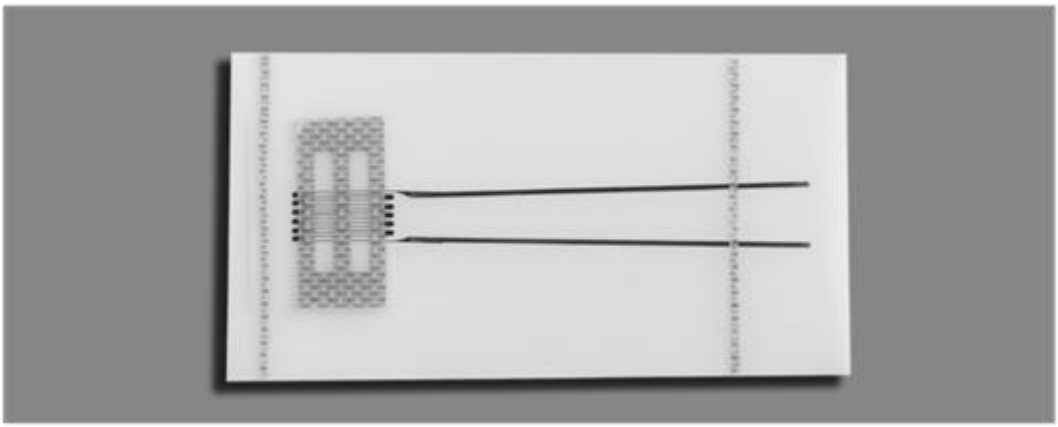

Figure 14. ZC-type High Temperature, Flame-Sprayed Installed Strain Gage available from Vishay. Nominal gage resistance of 120 ohms. Nichrome lead wires allow voltage output to be able to extend beyond perimeter of flame-spray.

5. THERMAL PROTECTIVE COATINGS FOR RESISTIVE STRAIN GAGES

Protective coatings were applied to a ZC-Series high temperature strain gages to dually insulate the gages and attach them to the substrate. The ZC-Series strain gage is an etched Kanthal (Fe-Cr-Al alloy) foil grid in free-filament form manufactured by Vishay Micro-Measurements Corporation, Wendell, NC (Figure 14). This product was sold by Vishay, Inc., specifically for application with a thermal spray coating. Vishay's recommended procedure involving a NiCrAl bondcoat and subsequent layers of Al_2O_3 to adhere and coat the strain gage was followed without success (Figure 15). Subsequently, a series of thermal spray coatings were applied in conjunction with high temperature strain gage cement. Variations of this approach were used to attach strain gages to the ½-inch diameter 304 SS tubing. In all cases, an Al_2O_3 coating was applied to the stainless steel substrate first. Then, the strain gage was attached to the underlying Al_2O_3 coating with high temperature cement. Finally, the cemented strain gage was coated over with a second layer of Al_2O_3. The SS tubing was then pressurized in a test apparatus which allowed strain gage response to be measured.

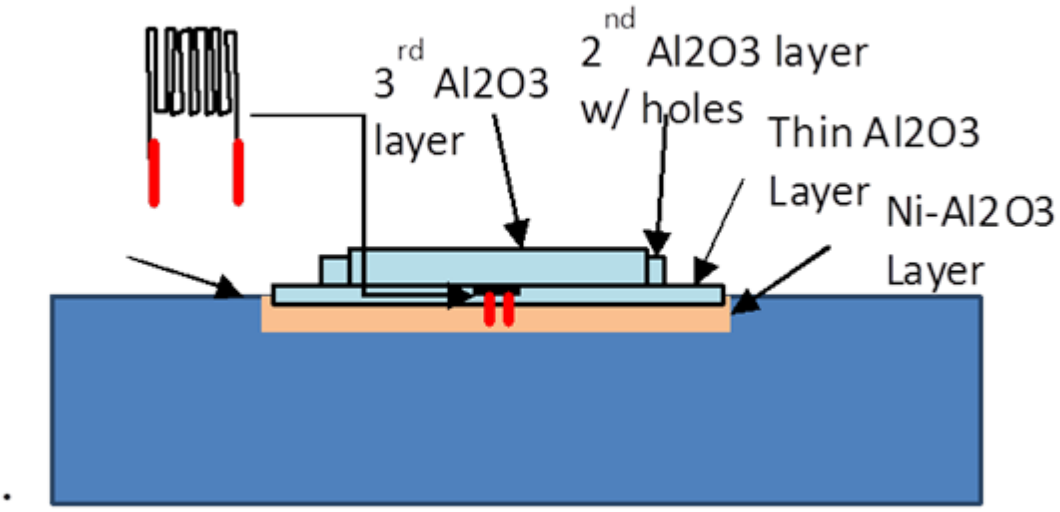

Figure 15. Strain Gage installation approach utilizing a thermal sprayed bondcoat and subsequent layers of Al_2O_3.

5.1. Gage on Grit Blasted Tube

Initially, the Vishay process for applying ZC strain gages was attempted. During this attempt the 6P Powder Flame Spray torch was used instead of the Rokide Torch used by Vishay. The Rokide torch is an oxy-acetylene torch that uses a ceramic rod as a feed stock instead of powder. It was felt that the 6P Powder Flame Spray torch operating on oxy-acetylene would produce a similar coating. The SS Tube was lightly grit blasted, then coated with a thin layer Al_2O_3 using the 6P Powder Flame set at the process parameters shown in Table 2, below.

Table 2. Spray Parameters for Al_2O_3 Flame Spray

Torch	Metco 6P
Powder	Praxair 101
Total Flow (TF) (SCFH)	90
Oxygen to Fuel Ratio (OFR)	2.0
Air Flow (AF) (SCFH)	90
Powder Gas Flow (PG) (SCFH)	10
Powder Feed Rate (PFR) (g/min.)	25
Standoff Distance (SD) (inches)	7.0
Traverse Rate (inches/s)	4
Passes	2

The ZC Gage (ZC-NC-61272-350) was then attached to the coated tube using the fiberglass tape provided with the strain gage. A second layer of Al_2O_3 was also applied. However, in all cases the fiberglass tape caught fire and melted the strain gage, as shown in Figure 16.

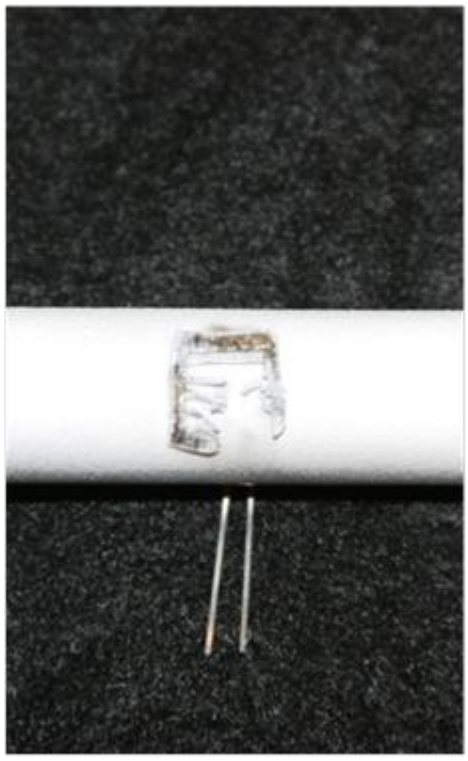

Figure 16. ZC-NC-61272-350 showing Melted Tape and Gage

In an attempt to reduce the heat load applied to the gage, standoff distances were increased, traverse speeds were increased, and a flame-cooling torch air cap was used. This resulted in the strain gage material surviving the spray process. However, the tape still caught fire. In all cases, it was nearly impossible to remove the fiberglass tape following the flame spray without damaging the strain gage. Because of this difficulty, and because of concerns about load transfer between the ceramic coating and the strain gage, this approach was abandoned in favor of high temperature strain gage cements. Cements provide improved adhesion between the gage and the tube before the overcoat of flame sprayed Al_2O_3 was applied, making it easier to remove the fiberglass tape.

It is believed that despite the similarities between the 6P and the Rokide torches, the longer standoff distance, smaller flame plume, and larger particle sizes associated with the Rokide torch contributed to the success reported by Vishay when using it to coat strain gages.

5.2. High Temperature Cements

Two high temperature strain gage cements were purchased from Vishay. Each cement was used to test strain gage application using the general approach shown in Figure 17. Two variations of this approach were also used. One involved a bond coat; the other involved cementing the strain gage directly to the stainless steel tube.

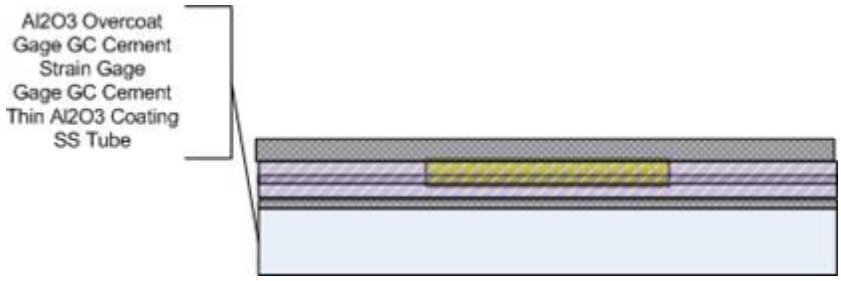

Figure 17. ZC-NC-61272-350 Schematic

5.2.1. GC Cement

The first cement was GC Cement rated to 1093°C. It had a high viscosity consistency, and was gray in color. The SS Tube was lightly grit blasted, then coated with a thin Al_2O_3 layer using the flame spray process. The tube was then masked and a layer of GC cement was applied using a brush; the gage was held in place using fiberglass tape. The assembly was then cured by heating to 93°C, holding for 30 minutes, then heating to 176°C and holding for another 30 minutes. The fiberglass tape was then removed after letting the assembly cool. Another layer of GC cement was applied and cured at 176°C for 30 minutes. An additional layer of flame sprayed Al_2O_3 was then applied over the GC cement. Due to the high viscosity and quick dry time of the cement, the finished strain gage / coating assembly was somewhat bulky (Figure 18).

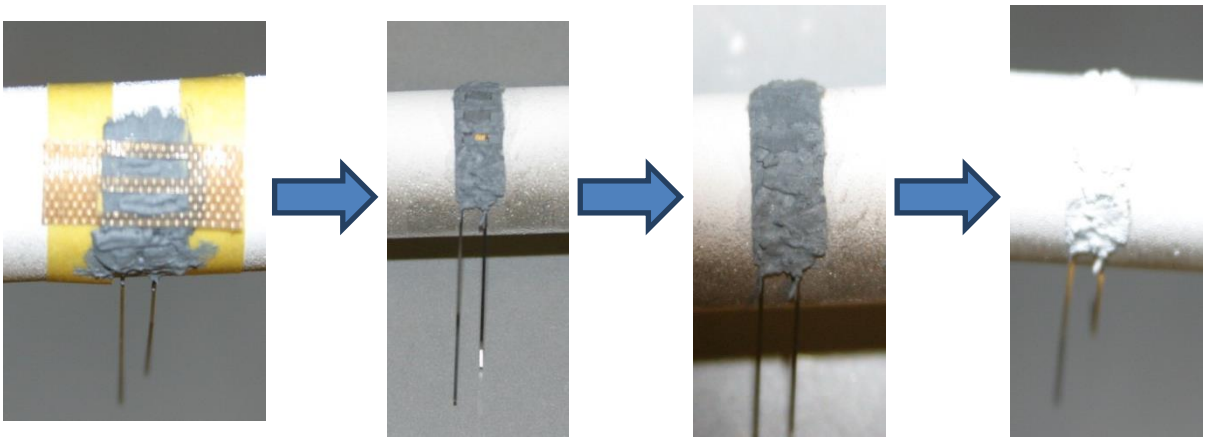

Gage Applied over cement

After Cure and Tape removal

Additional overcoat of GC applied

Flame Sprayed Al_2O_3 Over cement

Figure 18. GC Cement Strain gage application process

5.2.2. H Cement

The second high temperature strain gage cement tested was H Cement. It is rated to 870°C, has a low viscosity, and is green in color. The SS Tube was lightly grit blasted, then coated with a thin Al_2O_3 layer using the flame spray process. The tube was then masked and a layer of H cement was applied using a brush; the gage was held in place using fiberglass tape. The assembly was then cured by heating to 93°C, holding for 30 minutes, then heating to 176°C and holding for another 30 minutes. The fiberglass tape was then removed after letting the assembly cool. Another layer of H cement was applied and cured at 176°C for 30 minutes. An additional layer of flame sprayed Al_2O_3 was then applied over the H cement. Due to the lower viscosity of H cement, the application was not as bulky as GC cement and seemed to perform better (Figure 19).

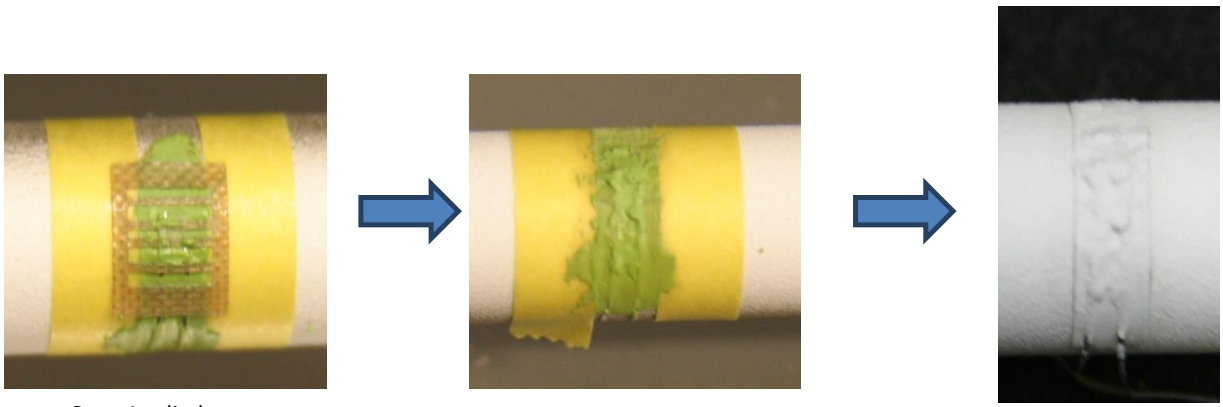

Gage Applied over H cement

After Cure Additional overcoat of GC applied

Flame Sprayed Al_2O_3 Over H cement

Figure 19. H Cement application process

5.2.3. Bondcoat with H Cement

A third sample was prepared by introducing a layer of Metco 443NS (72% Ni-18% Cr-6% Al) bondcoat material. The bondcoat was applied using the 6P powder flame spray torch directly onto the SS tube, as shown in Table 3, with no grit-blast surface preparation. In this case, the procedure described above was used to apply and cure the H cement and to secure the strain gage to the SS tube. An additional layer of Al_2O_3 was applied over the H Cement and the strain gage using the powder flame spray process (Figure 20, Figure 21).

Table 3. Parameters for Flame Sprayed Bondcoat

Torch	Metco 6P- K nozzle
Powder	Metco 443NS
Total Flow (TF) (SCFH)	131
Oxygen to Fuel Ratio (OFR)	1.67
Air Flow (AF) (SCFH)	100
Powder Gas Flow (PG) (SCFH)	10
Powder Feed Rate (PFR) (g/min.)	52
Standoff Distance (SD) (inches)	9.0
Traverse Rate (inches/s)	4
Passes	2

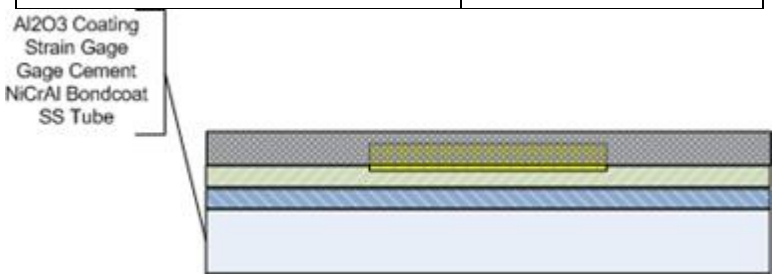

Figure 20. ZC-NC-61212-120 Strain Gage

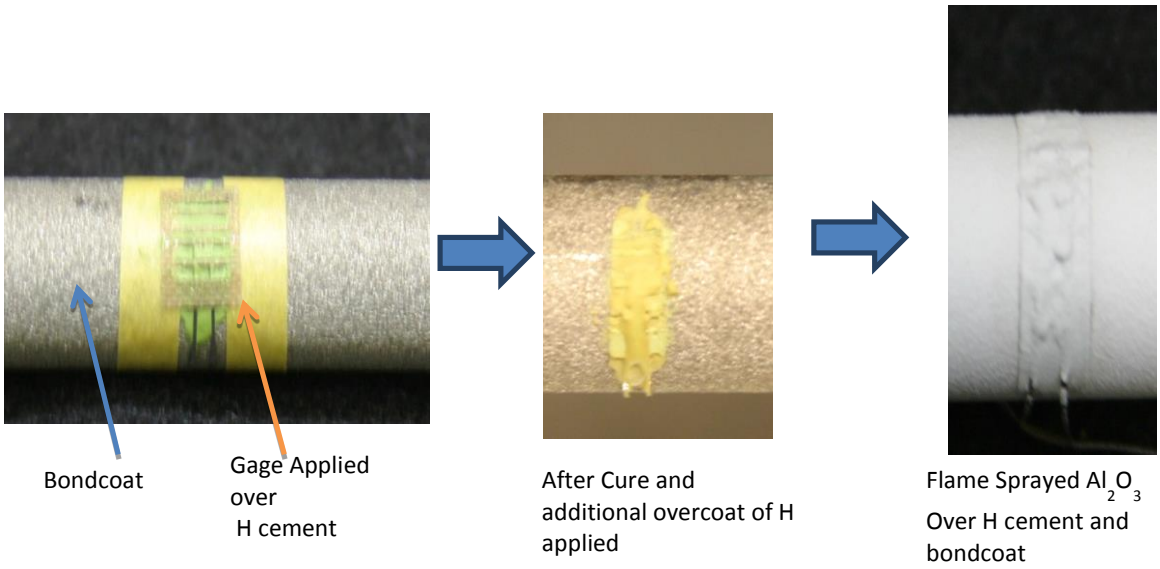

Figure 21. H Cement process with bond coat

5.2.4. Gage on bare SS Tube with H Cement

The last SS tube was prepared by attaching the strain gage directly to the tube using the H cement, Figure 22. The SS tube was cleaned and masked. Then, a layer of H cement was applied using a brush. The gage was held in place using fiberglass tape and cured at 93°C for 30 minutes followed by an additional bake at 176°C for 30 minutes. The fiberglass tape was removed after curing, Figure 23.

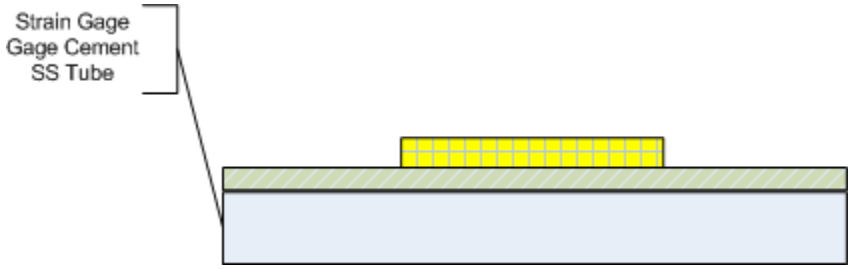

Figure 22. ZC-NC-61264-120 Strain Gage

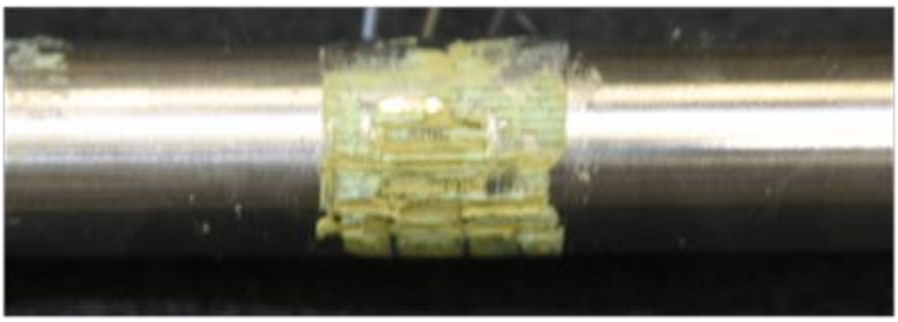

Figure 23. Strain gage applied on bare SS tube with H Cement

6. FLAME SPRAYED STRAIN GAGE TESTING

The ZC-type gages from Vishay were tested by pressurizing the tube and monitoring the strain gage response. Sample 1, GC Cement, was immediately discarded, because installation of the gage resulted in a change of the nominal resistance of 120 ohms. Sample 2, H Cement, was marked for testing, because it passed the initial screening for nominal resistance. It is a ZC-NC-G1262-120 gage (two wires). Sample 3, Bondcoat with H Cement, was immediately discarded, because installation of the gage resulted in a change of the nominal resistance of 120 ohms. Sample 4, Gage on bare SS Tube with H Cement, was marked for testing, because it passed the initial screening for nominal resistance. It is a ZC-NC-G1264-120 gage (four wires for temperature compensation). The two samples exhibited different coatings: the four-wire strain gage was covered in a green "shell-like" substance that was fracturing prior to testing, and the two-wire strain gage possessed a uniform white coating over the gage and pipe.

The initial test for the two remaining samples was an initial pressure test at 50 psig to ensure that the strain gages reacted to a stress on the substrate. During the first set of tests, the four-wire gage failed when one of the nichrome wires was severed close to the gage matrix during manipulation of the sample. It was, therefore, discarded for future tests.

Sample 2 survived the initial pressure tests due to a thicker outer coating and careful manipulation of the sample, both preventing the nichrome wires from becoming detached. The next set of fabrication verification and validation tests for the sample consists of measuring strain in the pipe as a function of temperature.

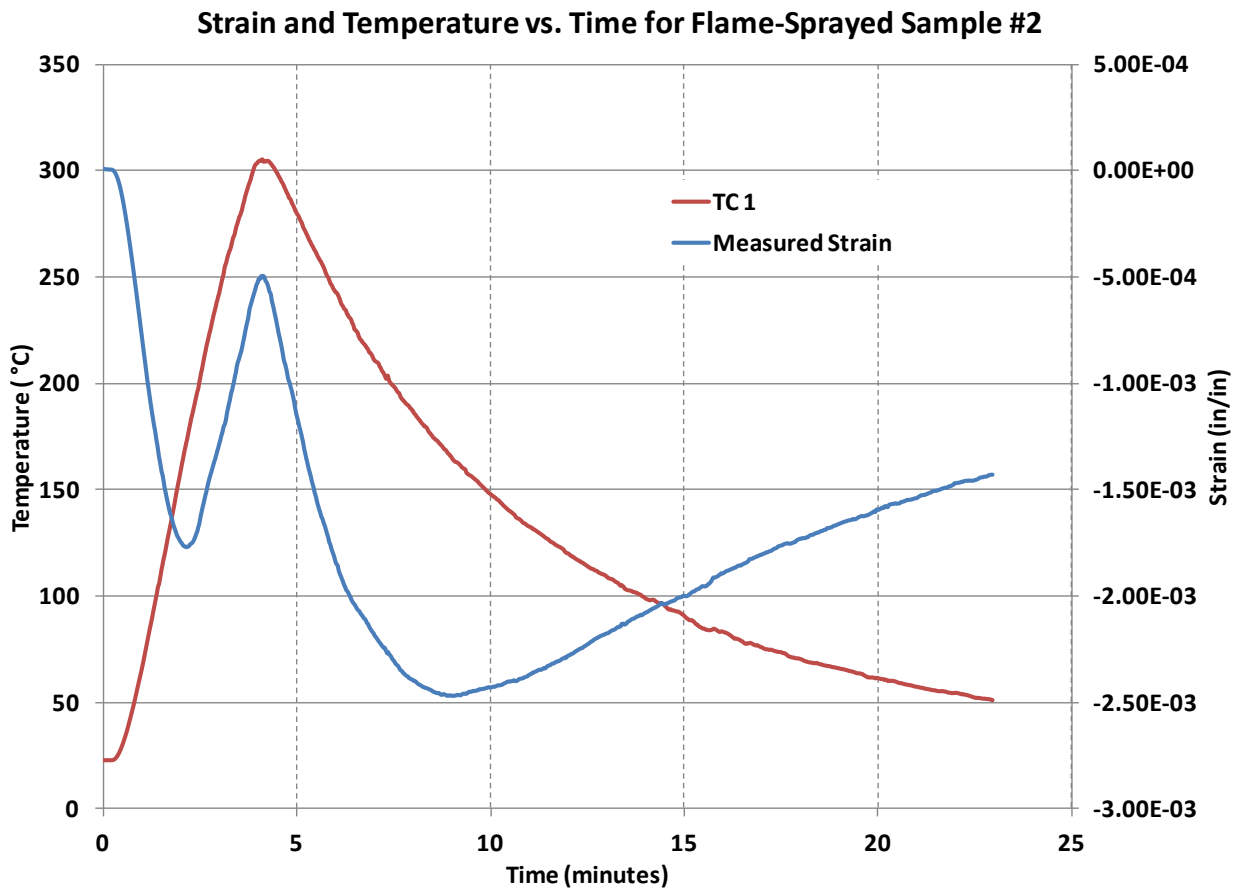

Figure 24. Correlation between Strain and Temperature for Flame-Sprayed Sample 2, Test 1

Figure 24 displays the data collected during the first temperature test for Flame-Sprayed Sample 2, Test 1. It is interesting to note the non-traditional relationship between temperature and strain. These results are discussed further in Figure 25, below.

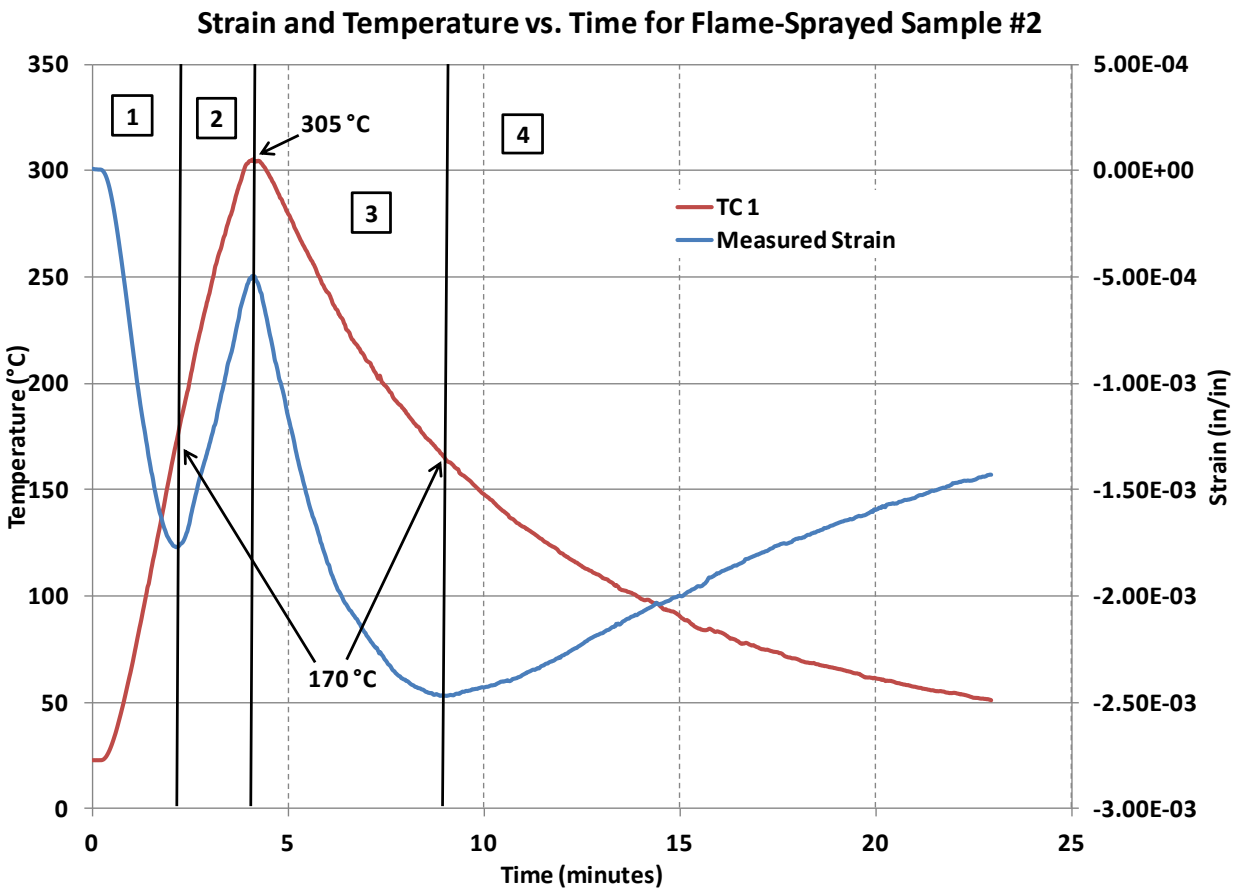

Figure 25. Important Points and Regions for Flame-Sprayed Sample 2, Test 1

Figure 25 depicts the same results as Figure 24, with several points and regions highlighted. To understand the operation of the strain in the material, it is important to understand the physics behind the flame-sprayed strain gage.

The flame-spray installed strain gage must be able to freely move without being constrained by the overall ceramic coating. In addition, the strain gage must be adequately adhered to the bonding layer of alumina flame-spray, which in turn must be adequately bonded to the stainless steel substrate. If the strain gage is constrained, an artificially negative strain is measured. Subsequently, if any bond between the strain gage, the flame-spray, and the substrate is compromised, then the strain gage will be decoupled from the substrate and an accurate measurement of strain for the material will not be possible. Recall Figure 25. The experimental results are discussed below in numerical order of the regions.

- Region 1: Heater turned on at 50% power. The strain gage shows negative strain (compression) due to constraint from the top coating of aluminum oxide ceramic. The negative strain aspect of the experiment will be explained in Figure 26.
- Region 2: Heater still at 50% power. The strain gage still shows negative strain, but at a reduced value. The beginning of region 2 is at 170°C. At this point, the coating is expanding faster than the strain gage, but it has not expanded enough to allow for

"unconstrained" expansion of the strain gage. This will occur at the "breakeven point" of zero measured strain.

- Region 3: Heater is turned off. The maximum temperature reached at the beginning of region 3 is 305°C. At this point, temperature decreases and strain is measured as more compressive. This is because the coating is contracting faster than the strain gage, creating an artificial strain signal.
- Region 4: Heater is still turned off. Temperature is still decreasing. However, once the temperature is 170°C, the strain gage measures a less compressive strain, because the coating has arrived at an expansion/contraction threshold. At this temperature of 170°C, the strain gage contracts faster than the coating, alleviating some of the compression force on the strain gage.

Figure 26 provides an insight as to how the non-constant thermal coefficient of expansion operates for the ceramic coating.

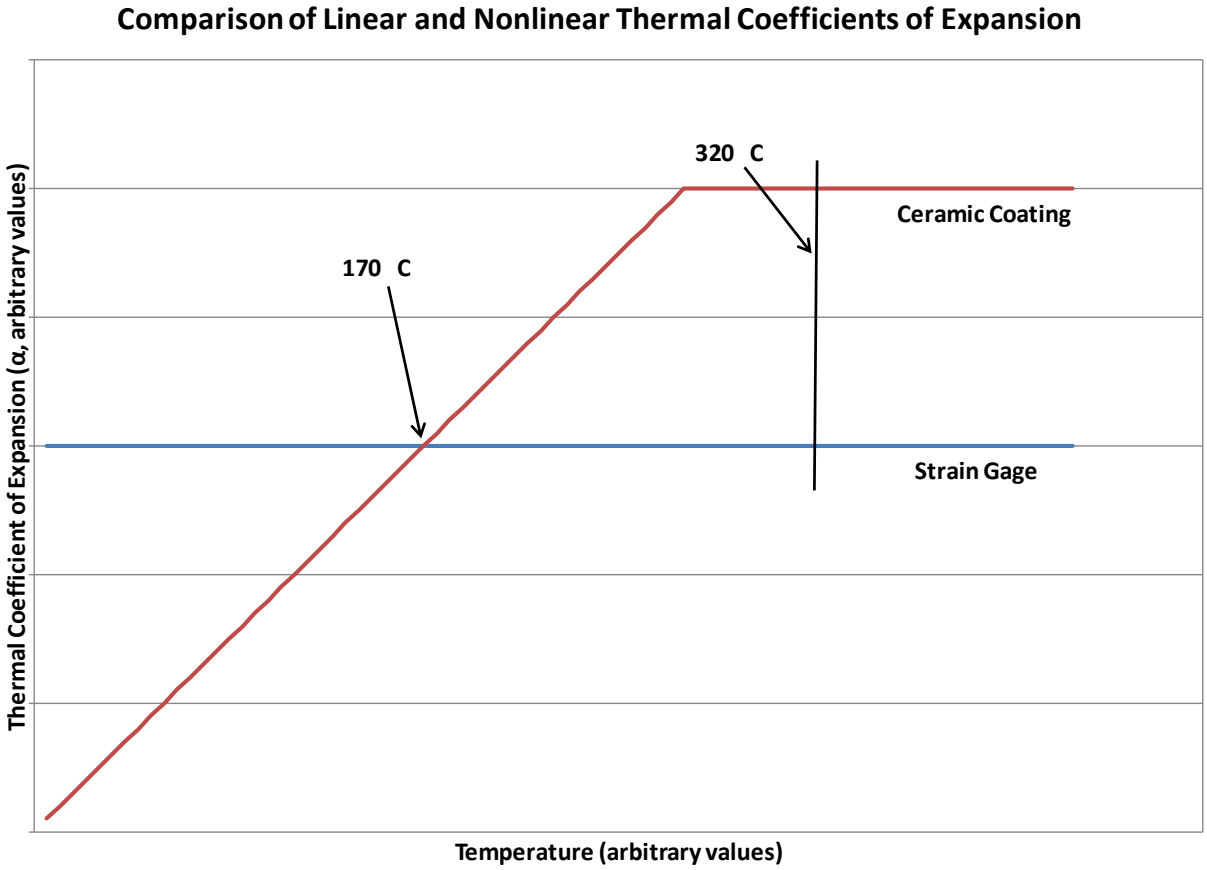

Figure 26. Comparison of Linear and Nonlinear Thermal Coefficients of Expansion for Ceramic Coating and Strain Gage on Sample #2. Figure is intended to be a pictorial representation rather than precise values.

The linear, non-constant thermal coefficient of expansion in the ceramic coating exists due to a unique condition of these types of thermal spray. As the thermal spray impacts the substrate, it forms a uniform, irregular coating over the strain gage. The coating naturally forms small cracks

within itself, which causes the linear thermal coefficient of thermal expansion. As the coating expands/contracts, the small cracks must deform/collapse for the material as a whole to deform. Though each crack deforms at a different temperature, a definite temperature can be determined at which the average crack in the coating has deformed. In this test case, the "crossover" temperature was 170°C. So, at 170°C, the compressive strain on the strain gage due to the ceramic coating is alleviated slightly, allowing the strain gage to more accurately measure the deformation of the stainless steel pipe. In addition, as temperature is increased, new cracks are formed, creating a sequence of "cold-activated" cracks and "hot-activated" cracks. This allows for a linear, non-constant α for the ceramic coating. Also, following the crossover point, there is a situation in which the relative position of the ceramic coating with respect to the strain gage is equivalent to the initial position of the test sample. This occurs at a temperature of approximately 320°C in the experiment. Past this point, all deformation measured by the strain gage is uninfluenced by the ceramic coating and is, instead, a true measurement of strain. This would indicate that flame-sprayed strain gages have a minimum threshold at which they are useful to an experimenter. Mathematically, the strain measured by the strain gage as a result of the influence of the ceramic coating can be represented as:

$$\varepsilon = \int_{coating} \alpha dT - \int_{gage} \alpha dT$$

Therefore, at temperatures below 170°C, the strain is negative, due to compression from the ceramic coating. Likewise, a "breakeven" point of zero strain occurs at 320°C, at which the two integrals are equivalent. So, true strain can only be identified past the "breakeven" point. In addition, if the coefficient α is assumed to be constant for the strain gage, measured, unconstrained strain will be given by the simplification of the integral

$$\varepsilon_{gage} = \alpha_{gage} T,$$

assuming the ceramic coating no longer imparts pressure on the gage past the "breakeven" point. This is equivalent to the strain induced only by temperature in a cylindrical pipe, matching textbook references.

The next test set was similar to the first, but more extensive, repeating the heat-up and cool-down phenomenon. Figure 27 shows the raw data from the experiment. Figure 28 displays Figure 27 in a more detailed fashion.

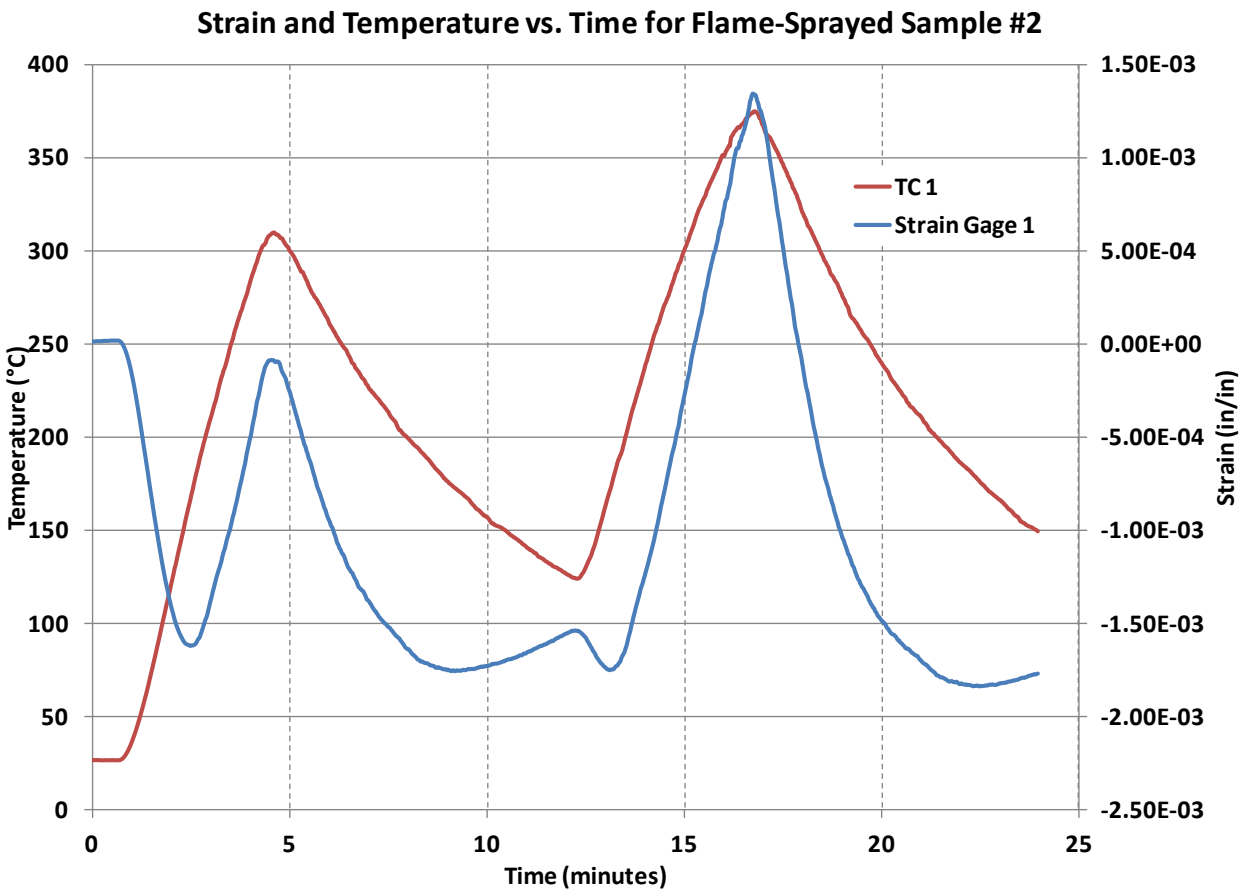

Figure 27. Correlation between strain and temperature for Flame-Sprayed Sample #2, Test 2.

As also indicated in Figure 24, it is interesting to note in Figure 27 that there is a non-conventional relationship between strain and temperature of the sample. Figure 28 displays significant regions and local phenomena in an effort to understand the mechanical interactions between the strain gage and the ceramic coating during these tests.

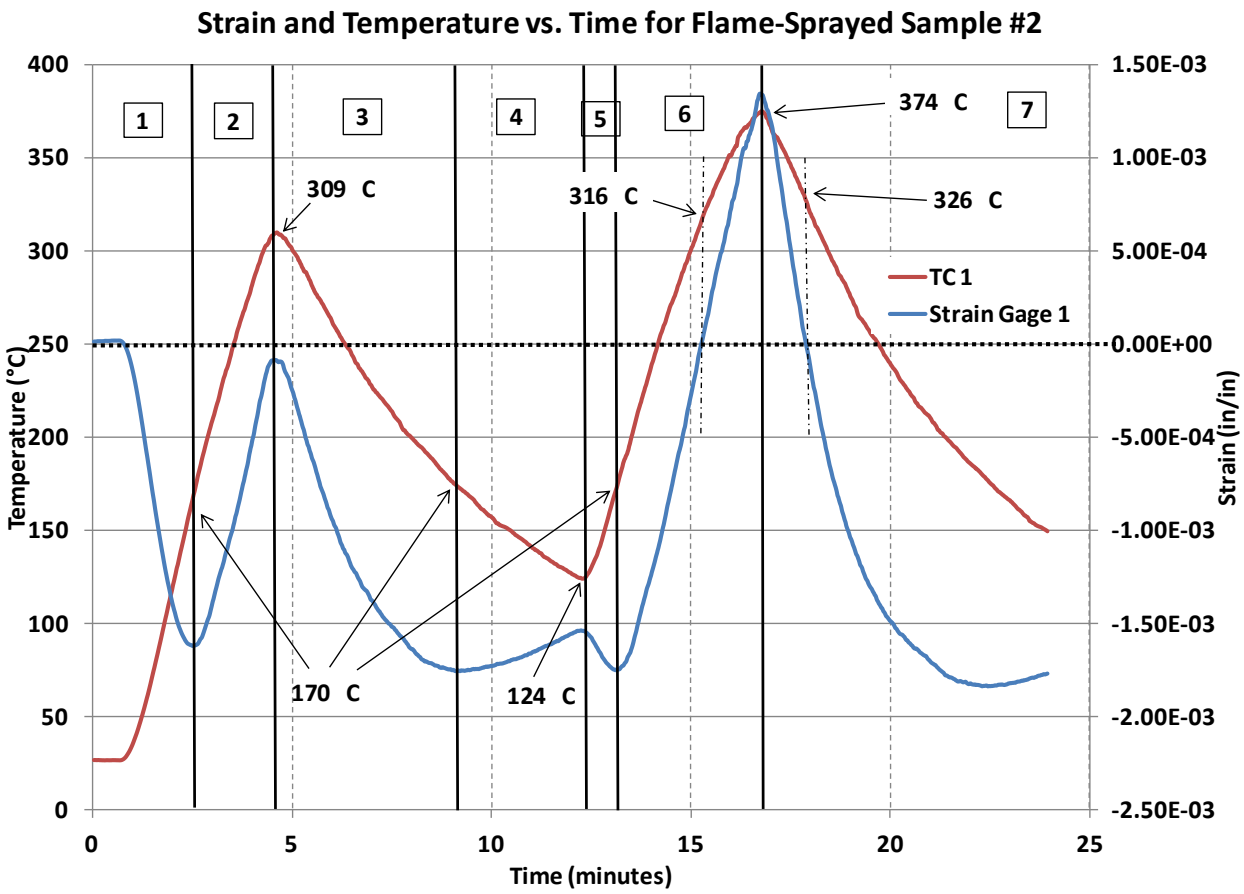

Figure 28: Important Points and Regions for Flame-Sprayed Sample #2, Test 2.

Figure 28 provides a detailed analysis of the raw data from Test 2 of Sample #2 based on regions in the data. The results and phenomena observed are:

- Region 1: Heater turned on at 50% power. The strain gage shows negative strain (compression) due to constraint from top coating of aluminum oxide ceramic coating. The negative strain aspect of the experiment will be explained in Figure 26.
- Region 2: Heater still at 50% power. The strain gage still shows negative strain, but at a reduced value. The beginning of region 2 is at 170°C. At this point, the coating is expanding faster than the strain gage, but it has not expanded enough to allow for "unconstrained" expansion of the strain gage. This will occur at the "breakeven point" of zero measured strain (shown by the horizontal dotted line on the graph).
- Region 3: Heater is turned off. The maximum temperature reached at the beginning of region 3 is 309°C. At this point, temperature decreases and strain is measured as more compressive. This is because the coating is contracting faster than the strain gage, therefore creating an artificial strain signal.
- Region 4: Heater is still turned off. Temperature is still decreasing. However, once the temperature is 170°C, the strain gage measures a less compressive strain because the coating has arrived at an expansion/contraction threshold. At this temperature of 170°C, the strain gage contracts faster than the coating, alleviating some of the compression force on the strain gage.

- Region 5: At 124°C, the heater is turned back on to 50% power. Strain gage expands quickly, causing a negative strain measurement.
- Region 6: This continues until 170°C, where the previously discussed phenomenon dominates and the strain gage begins to be less "constrained" by the ceramic coating. At about 316°C, the "breakeven" point is reached, where zero strain is measured. Any measurements made at temperatures greater than the "breakeven" temperature can be considered a true strain measurement.
- Region 7: At 374°C, the heater is turned off, allowing the sample to cool. The temperature of sample #2 decreases below about 326°C, crossing back across the "breakeven" point. At this point, the strain measurement is artificial, caused by the constraint of the ceramic coating.

The second test on Sample #2 distinctly illustrates that the results from Test #1 are not a fluke, but are, instead, true measurements. These measurements are used to support a hypothesis about the coefficient of thermal expansion for the ceramic coating with respect to the strain gages.

Therefore, the main conclusion from this testing is the fact that the strain gages are not constrained by the ceramic coating past a threshold of about 320°C. Therefore, this kind of high-temperature application may be suitable for the flame-spray technology.

Further test results (tests #3-5) are available upon request. They have been omitted here, because they describe the same phenomenon and would illustrate redundant concepts.

7. OPTICAL STRAIN MAPPING

An optical strain mapping approach was also investigated. Stainless steel tubes were coated to produce a two-tone color effect with the goal of being able to use image mapping software to deduce a strain relationship for a fuel cell rod application (Figure 29, Figure 30). Two different material sets were used to demonstrate feasibility on ½-inch SS tubes: a 70% Al-30% Cu powder blend, and a layered coating approach using Al_2O_3 and a 70%Al_2O_3-30% TiO_2 blend. All of these coatings were prepared using the Triplex Air Plasma Spray torch.

Figure 29. Picture of four tubes at varied coating conditions

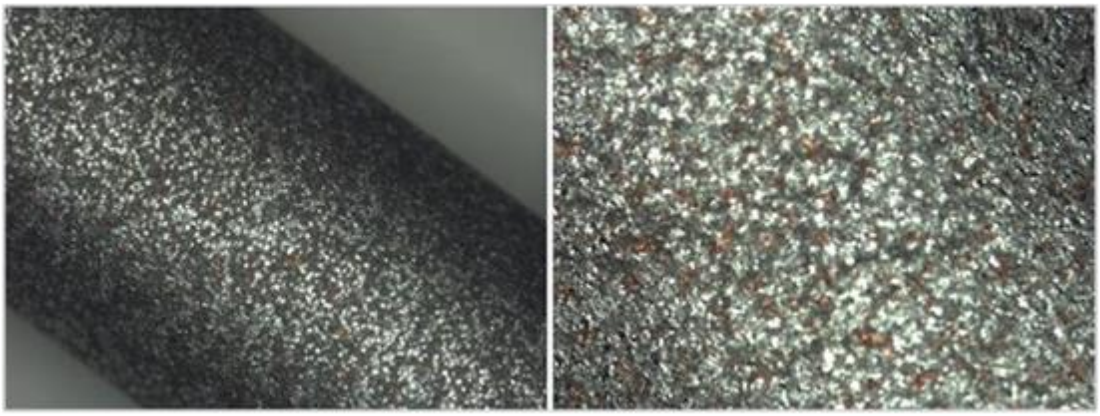

Figure 30. Close up view of two-color Al-Cu coated tubes for strain mapping

Four tubes were sprayed with the Cu-Al blend. The associated process parameters are shown in Table 4. Amperage was varied to try to improve the degree of melting of the copper particles

present on the coating, and the number of passes of over the part was varied to change coating thickness.

Table 4. Process Parameters for Al-Cu Parts

Tube #	AMPS	Ar	He	Feed Rate (lbs/hr)	Powder Gas (SCFH)	Hopper (PSI)	Vibration (PSI)	Standoff (in)	Traverse Speed	# Passes
1	300	150	10	2.65	10.6	4.4	5	6	999	3
2	350	150	10	2.65	10.6	4.4	5	6	999	4
3	400	150	10	2.65	10.6	4.4	5	6	999	4
4	350	150	10	2.65	10.6	4.4	5	6	999	1

Three tubes were sprayed with two powders feeders using an Al_2O_3 and a 70%Al_2O_3-30% TiO_2 blend (Figure 31, Figure 32). Tube #1 was sprayed using the same approach as for the Cu-Al tubes, utilizing a 70%Al_2O_3-30% TiO_2 blend with one powder feeder, however these coating resulted in a gray mono-tone color. As a result, a layered approach was used to coat tubes #2 and #3. These tubes were sprayed with pure Al_2O_3 first, and then a final coating pass was applied using the 70%Al_2O_3-30% TiO_2 blend. The associated process parameters are shown in Table 5. Only the number of passes of over the part was varied.

Table 5. Process Parameters for Al_2O_3-TiO_2 Parts

				Hopper #1 Al203				Hopper #2 Al203-TiO2 Blend					
Tube #	AMPS	Ar	He	Feed Rate (lbs/hr)	Powder Gas (SCFH)	Hopper (PSI)	Vibration (PSI)	Feed Rate (lbs/hr)	Powder Gas (SCFH)	Hopper (PSI)	Vibration (PSI)	Traverse Speed	# Passes
1	520	91.3	45	2.6	12	4	10	1	14	4	15	999	2
2	520	91.3	45	2.6	12	4	10	1	14	4	15	999	2+1
3	520	91.3	45	2.6	12	4	10	1	14	4	15	999	3+1

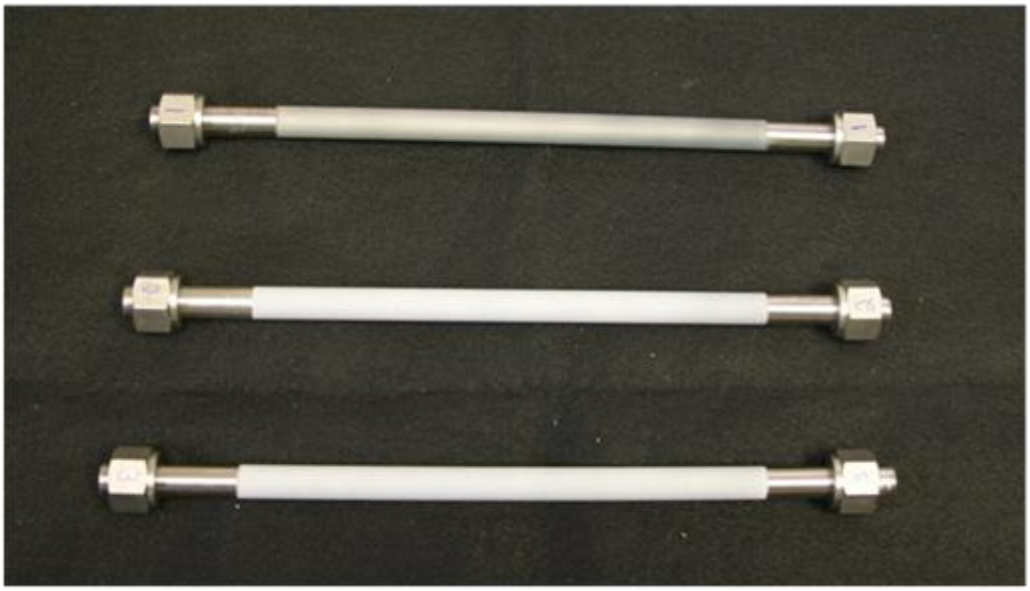

Figure 31. Picture of three Al_2O_3-TiO_2 tubes at varied coating conditions

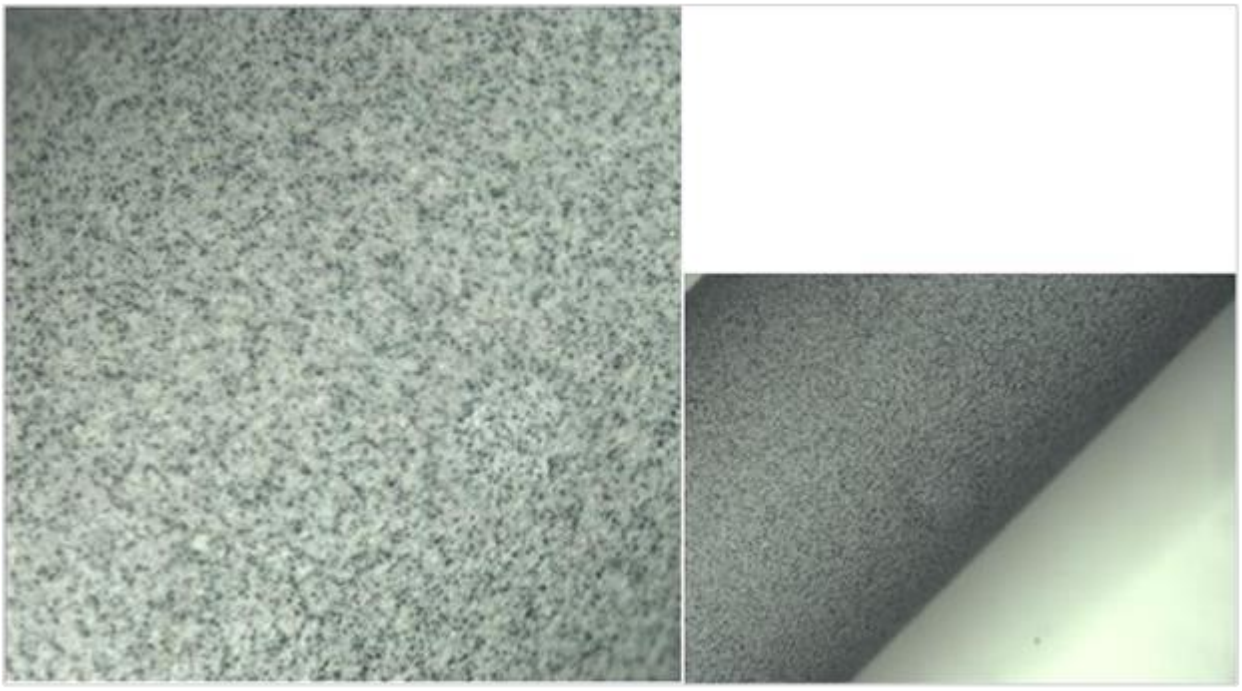

Figure 32. Close-up view of Al2O3-TiO2 tubes showing two-tone color for strain mapping

This initial step has been successful in developing a two-tone colored coating ("speckle coating") with two different material sets that may be appropriate for strain image mapping. In addition, if other materials sets are needed, it is believed that most materials that might be suited to a fuel cell rod application can be blended and coated using the Triplex air plasma spray system.

This alternative to traditional resistive gages is a varied and developing area of scientific research, which is still in its adolescence when compared to the vast knowledge associated with "traditional" resistive strain gages.

7.1. Digital Image Correlation (DIC)

Recent advances, such as the thermal spray speckle coating method described in the previous section, allows measurement of strain without a resistive bonded gage. In this technique, an array of dots or lines is burnished onto the sample and this area of the sample is continuously monitored during the experiment. As strain in the sample occurs, the configuration of the dots and lines is altered. This technique does require a pseudo-shunt calibration to determine an initial dot position, allowing for a correct strain value to be calculated from a difference in dot position.

The incorporation of optical strain mapping into a computationally-driven strain calculation leads to a current area of Sandia research called Digital Image Correlation (DIC). The DIC software computes the relative motion of the "speckles" on the test specimen, calculating the strain in the process during each time step.

The "coating" fills in the grain boundaries of the sample. The DIC cameras and software are able to recognize the material surface's "change in pattern," allowing a strain value to be measured.

8. SECOND ACRR PULSE SHOT

To feasibly use DIC to determine strain on fuel cladding during operation at ACRR, the instrumentation used must be able to survive reactor environments for sustained periods of time. The instruments of concern include the camera(s) used for optical mapping, cables, and light sources. To define the extent of radiation damage received by each of these pieces of equipment, an experimental test package was fabricated to place in the central cavity of ACRR, similar to the first ACRR test discussed in this report.

The second pulse experiment within the ACRR central cavity occurred on 14 August 2012. The experiment was designed to test the feasibility of using a borescope consisting of four separate lenses to extend the range of an optical camera, thereby lessening radiation effects from the reactor.

The package was equipped with a single Zircaloy-4 cladding sample, which had a small area of speckle pattern. In addition, a Vishay strain gage was attached to the bottom of the cladding sample to verify any strain results from the DIC. The optics for the experiment included a single radiation-hardened camera, set up to visualize the sample through the borescope lenses, and two small cameras placed at different heights on the package to determine the radiation effects on the cameras. Figure 33 depicts the experimental test package for the second ACRR test.

The central cavity in ACRR does not allow ambient light to reach the testing area during operation of the reactor, courtesy of a radiation shield plug that fills the cavity behind the testing package. Because of this, three different types of 120-volt light sources were installed into the package to produce light for the cameras. However, these light sources are susceptible to

radiation damage. The halogen lamp proved to be the most robust light source, lasting longer than either the incandescent bulb or the LED light.

However, by using Thermal Spray Coatings coupled with DIC software, both of the major issues presented in this section are effectively avoided, due to optical, rather than electrical measurement. In addition, the Thermal Spray Coating provides a more robust "attachment" to the substrate, because there is no foil backing to degrade and decrease measurement sensitivity to a resistive-type foil strain gage.

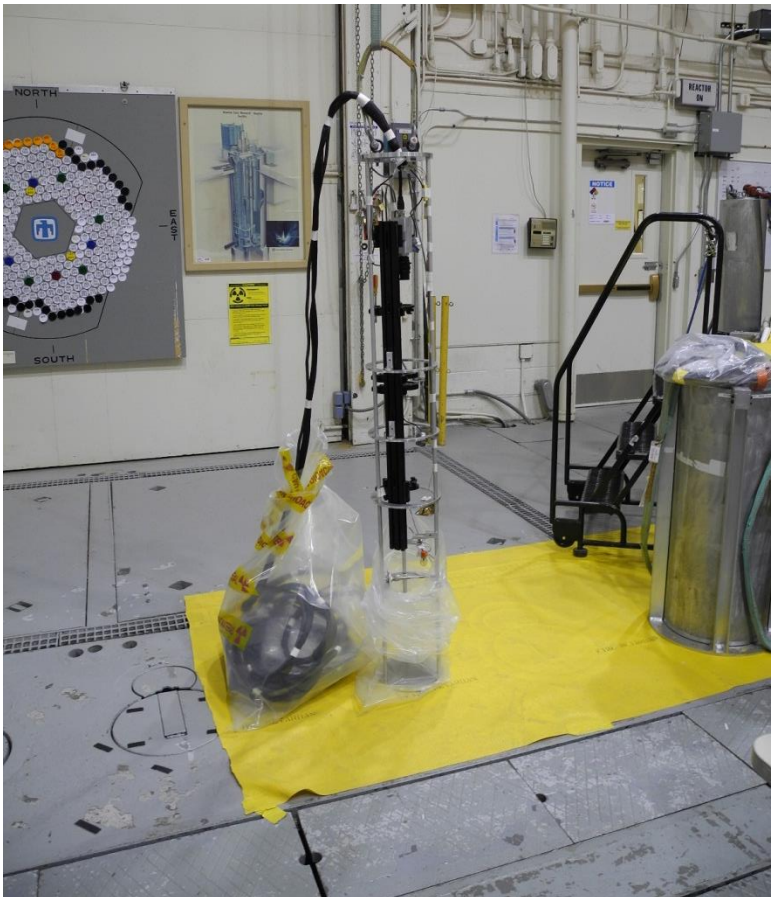

Figure 33. Test Package for ACRR shot on 14 August 2012

At the beginning of the test, the cameras were turned on to ensure proper function. Figure 34 depicts the image captured at the bottom of the central cavity prior to the reactor operation. It is important to note the clarity of the image: the speckled dots are readily identified.

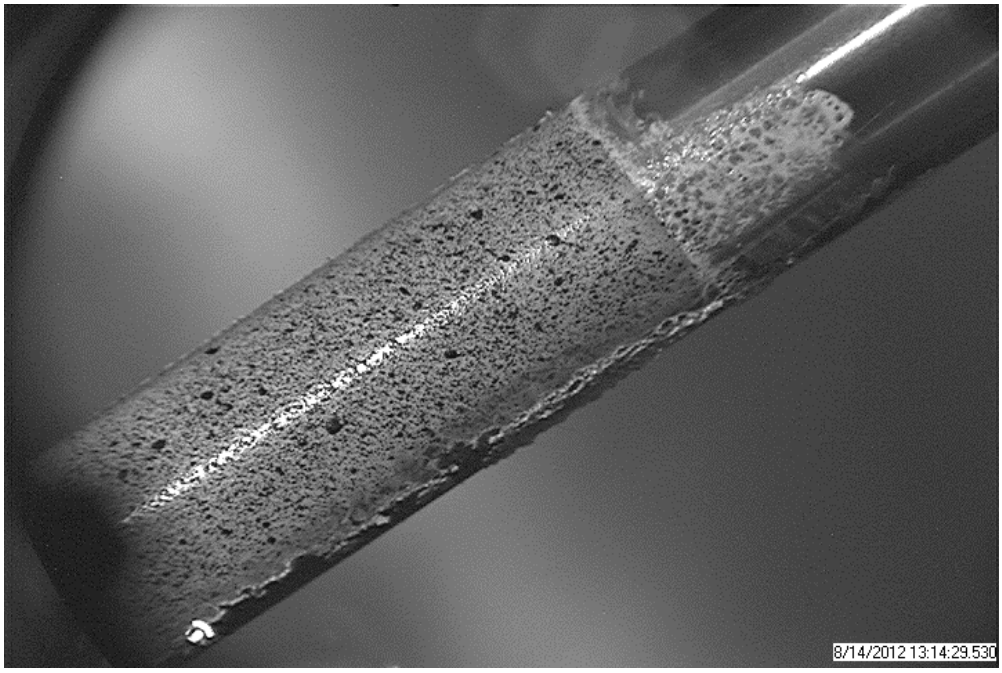

Figure 34. Beginning of ACRR steady-state test. View from the rad-hard camera through the four borescope lenses.

As the control rods are moved out of the reactor, the reactor increases in steady-state power. The radiation effects are evident in Figure 35; the white specks emerge onto the image as photons and neutrons interact with the camera and lens material. Figure 36 and Figure 37 show that the speckles due to radiation increase with increased steady-state reactor power.

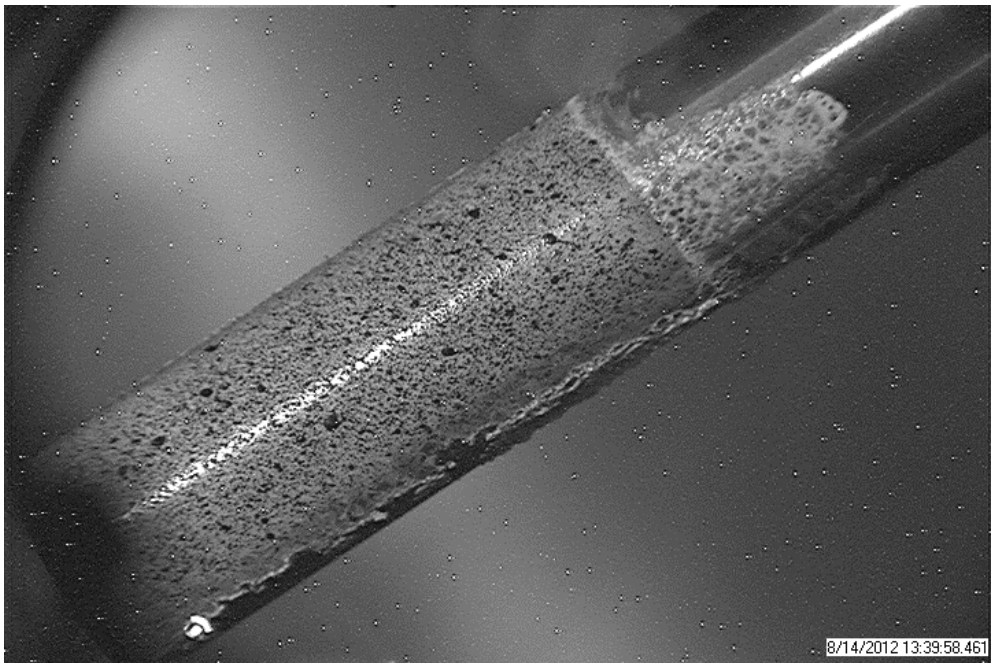

Figure 35. Very low reactor power. White speckles are beginning to appear.

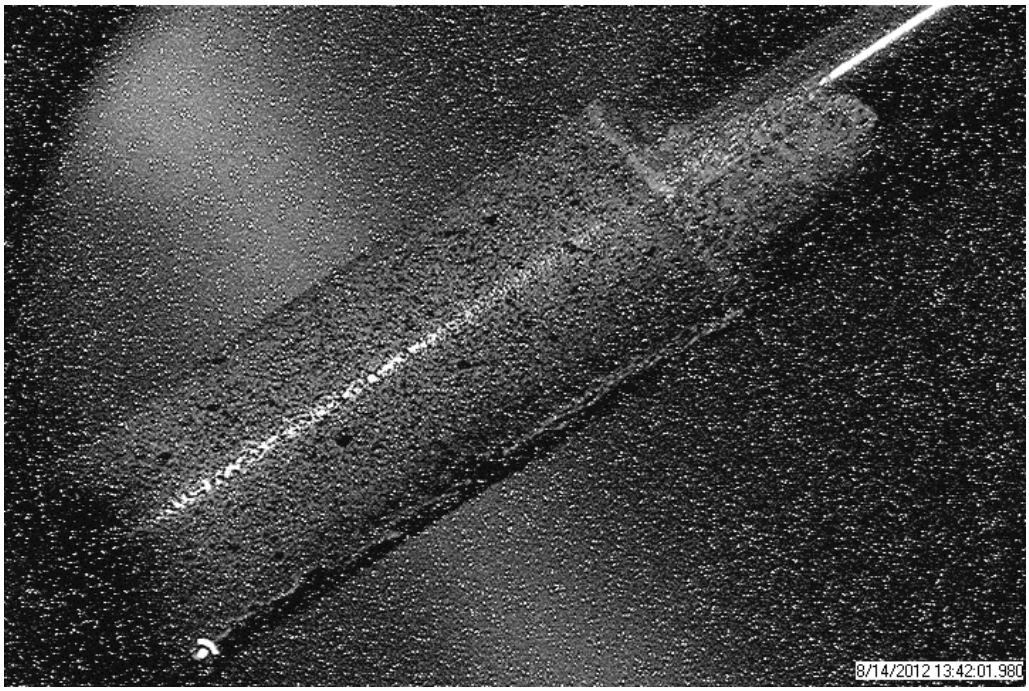

Figure 36. Approximately 2% steady-state power. White specks continue to appear.

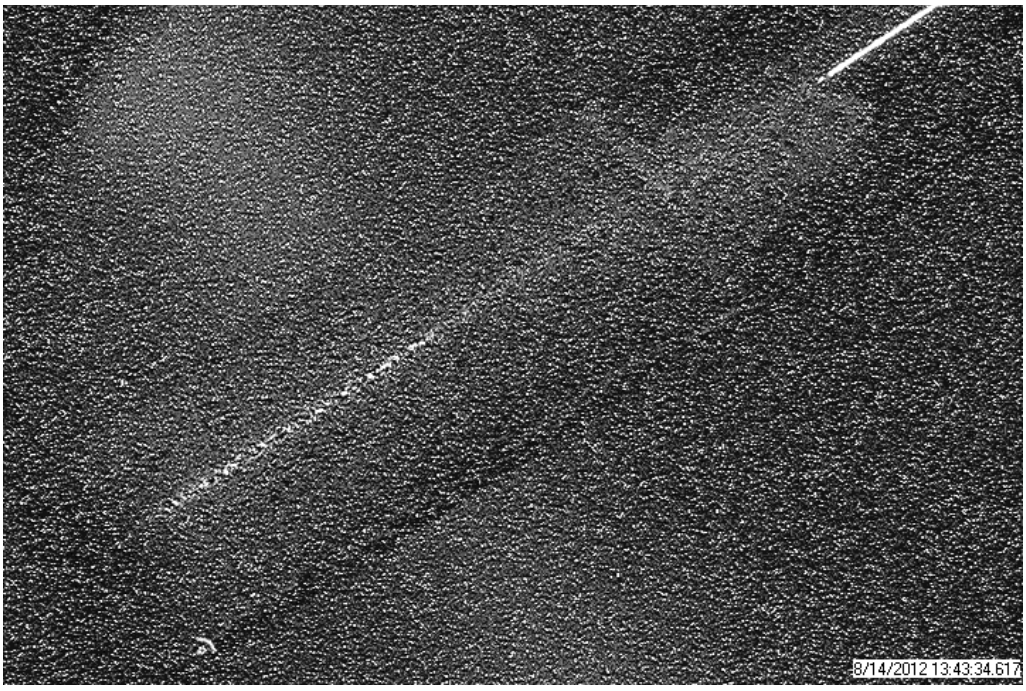

**Figure 37. Approximately 5% steady-state power.
White specks disrupt the image greatly.**

In addition, the light source in Figure 35 through Figure 37 is decreasing in brightness as reactor power is increased. These figures are seen with the incandescent bulb. Therefore, the radiation has negative effects on the incandescent light bulb's brightness.

Reactor power is then decreased, because the speckles caused by radiation are too numerous to accurately see the test specimen. Figure 38 shows the test specimen when reactor power is lowered back to 2% steady-state power.

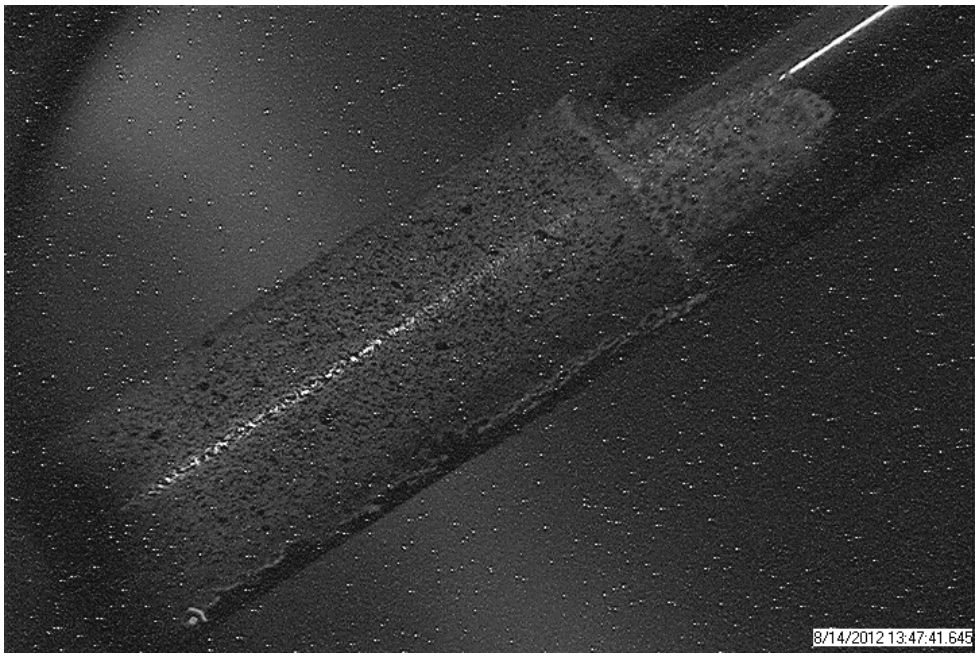

Figure 38. Reactor power is decreased to approximately 2%. White speckles are decreasing in quantity.

In Figure 39, reactor power is then increased again, moving up to 9.5% of steady-state power. The white speckles obscure nearly the entire test specimen. The incandescent light bulb is nearly out due to the radiation effects.

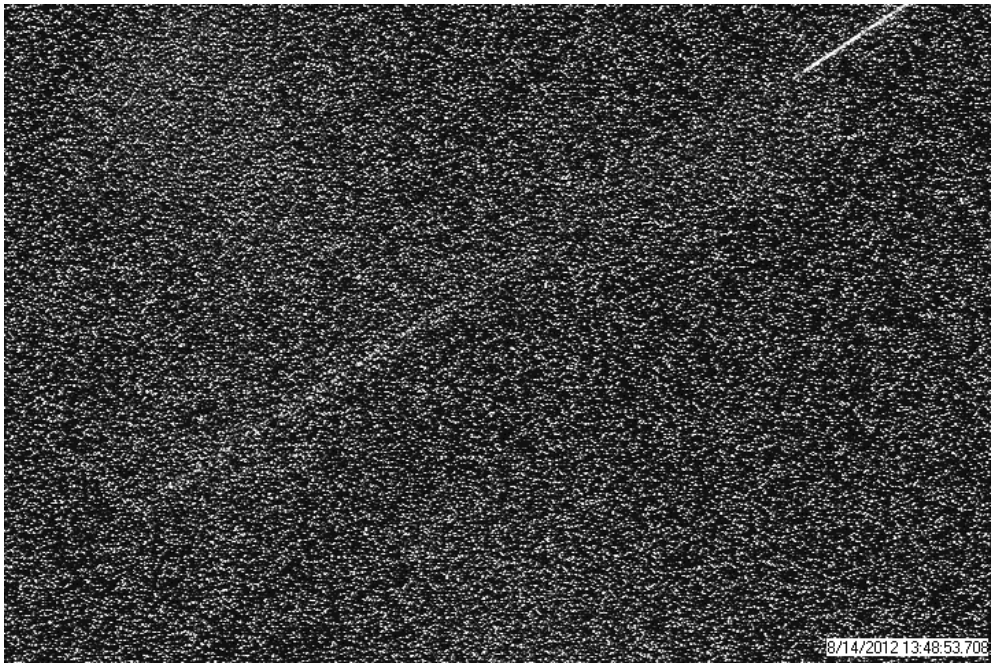

Figure 39. Reactor at 9.5% steady-state power. White speckles increase substantially.

At this point in the experiment, the incandescent light is turned off, and the halogen lamp is turned on to contrast the light sources' reaction to radiation. Figure 40 shows that the halogen lamp provides a brighter light than the incandescent light bulb at this level of radiation.

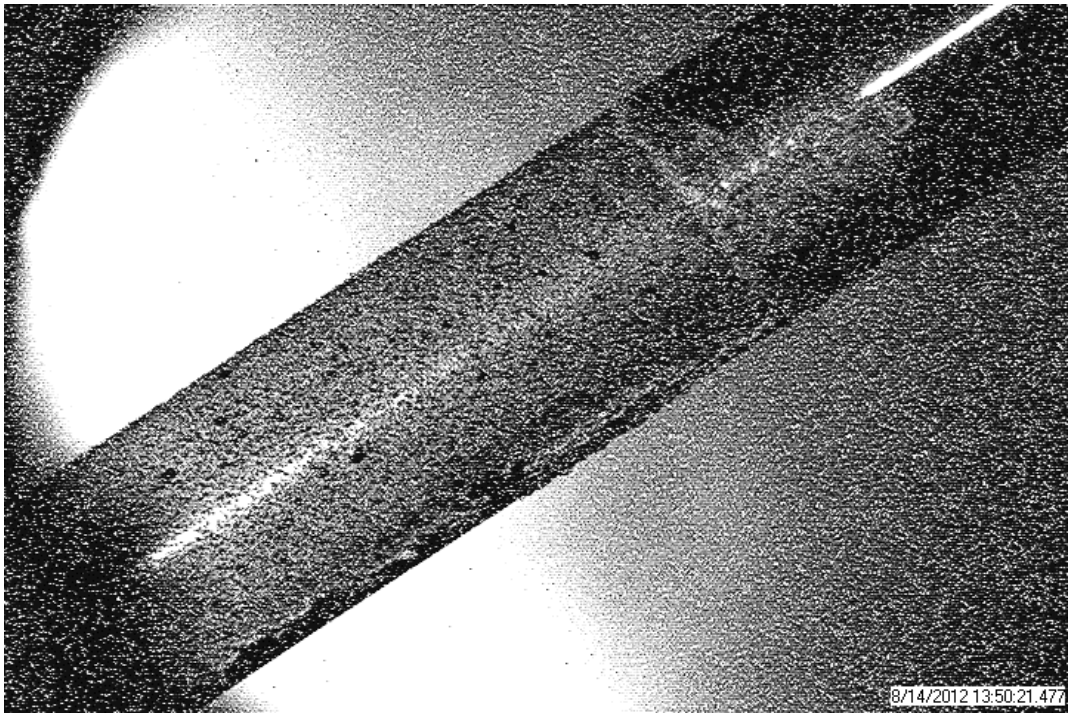

Figure 40. Reactor power at 9.5% steady-state power with halogen lamp as light source.

Next, the LED light is turned on to compare its light intensity to the light provided by the other two light sources. Figure 41 and Figure 42 show that the LED performs well, as compared to the incandescent light bulb. At approximately 14:02, all control rods were inserted into the reactor, shutting down the steady-state test. The vast difference in Figure 41 and Figure 42 is due to this event.

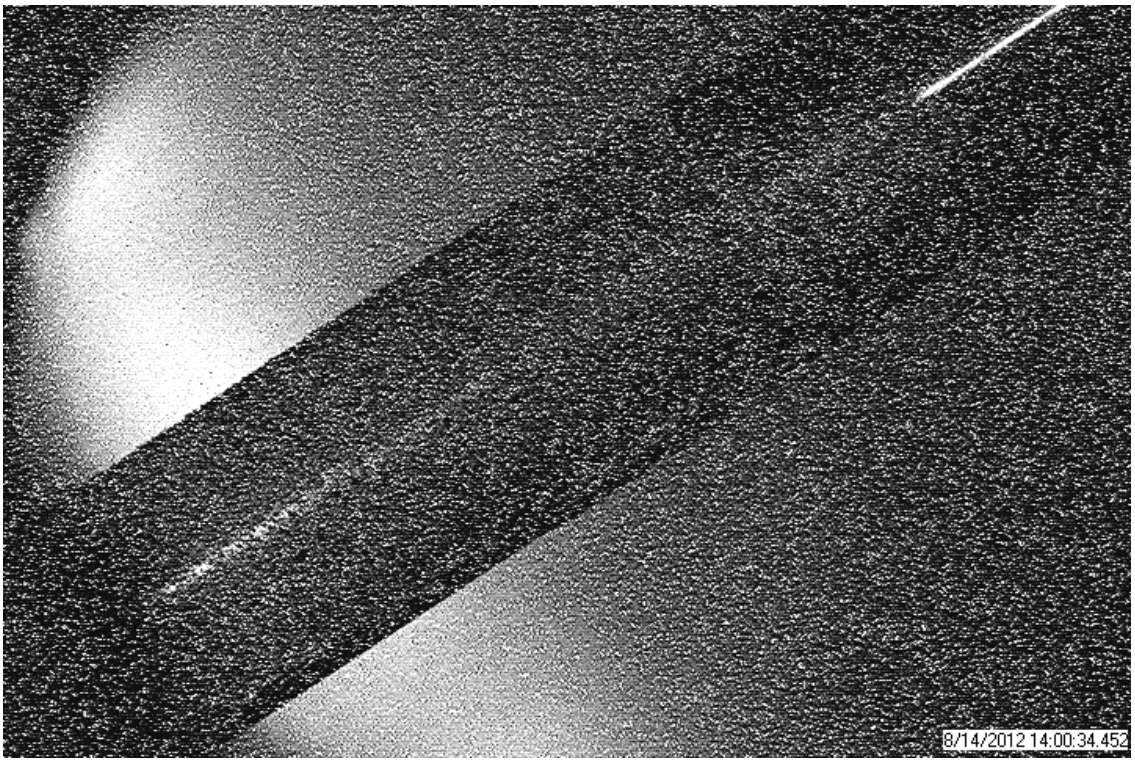

Figure 41. Reactor at 9.5% steady-state power with LED as light source.

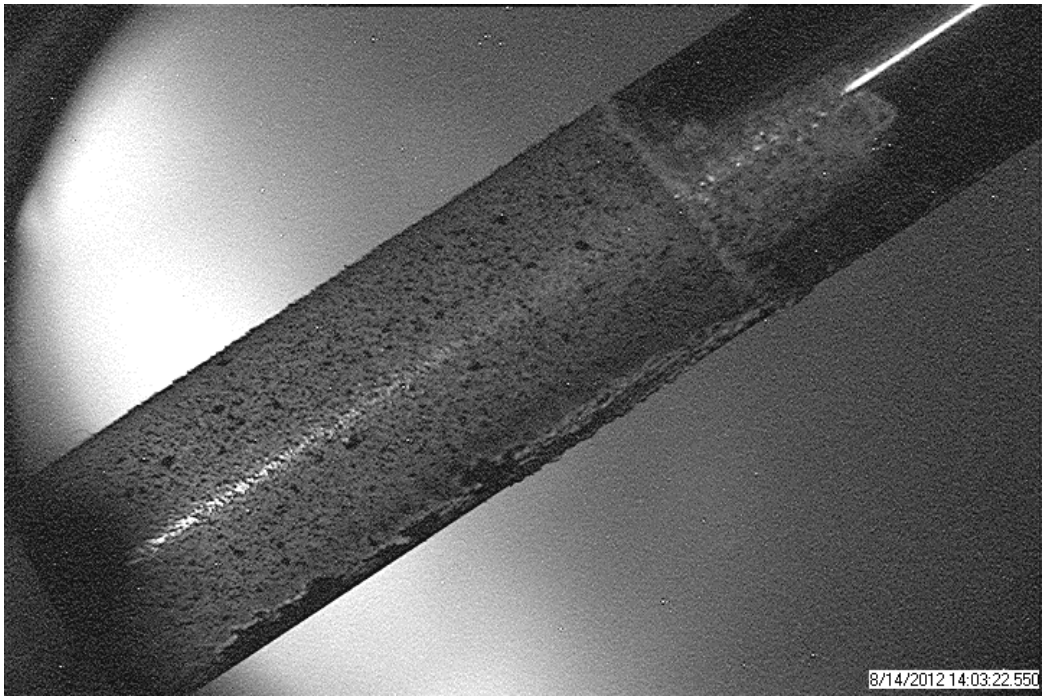

Figure 42. Reactor at very low power with LED as light source.

Figure 43 displays the same image as Figure 42, but with the incandescent light bulb as the light source. The test specimen can barely be identified. As a result, future ACRR optical strain mapping experiments will not use an incandescent light as the light source.

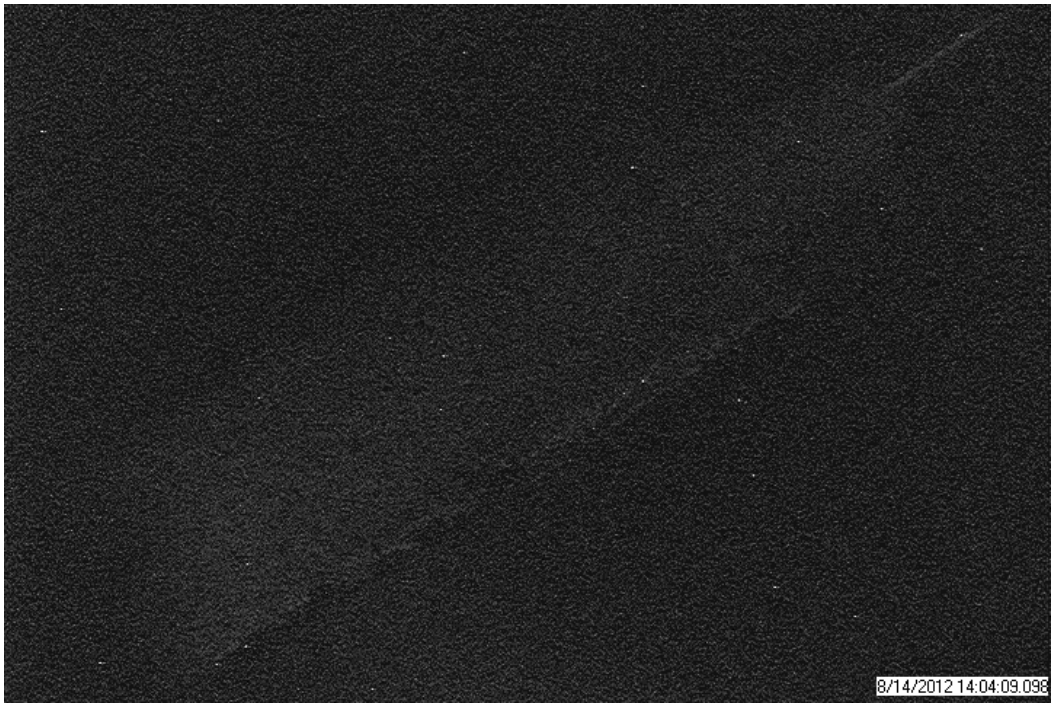

Figure 43. Reactor at very low power with incandescent light bulb as light source.

At this point, the halogen lamp was turned back on, depicted in Figure 44, highlighting the difference between the best and worst light sources when compared to Figure 43.

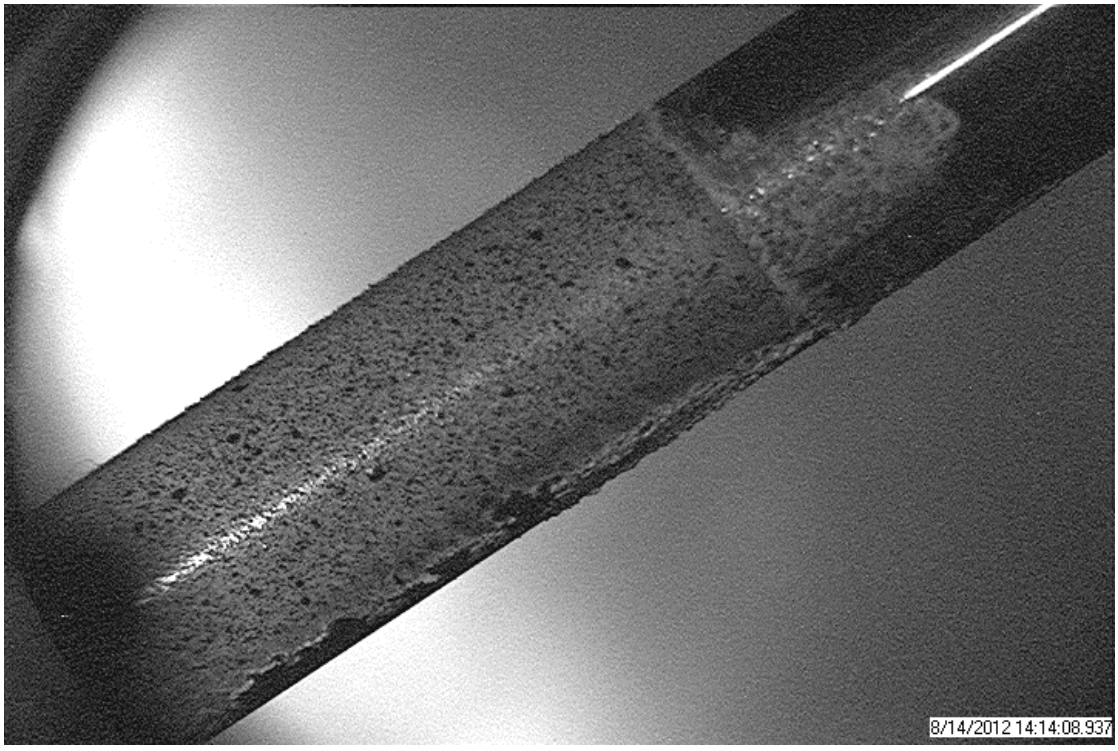

Figure 44. Reactor at very low power with halogen lamp as light source.

The power data displayed in Figure 45 gives an indication of the reactor characteristics during the test. The first "hump" represents a rise to 5% of maximum steady-state power, while the increased, longer power plateau represents 9.5% of maximum steady-state reactor power.

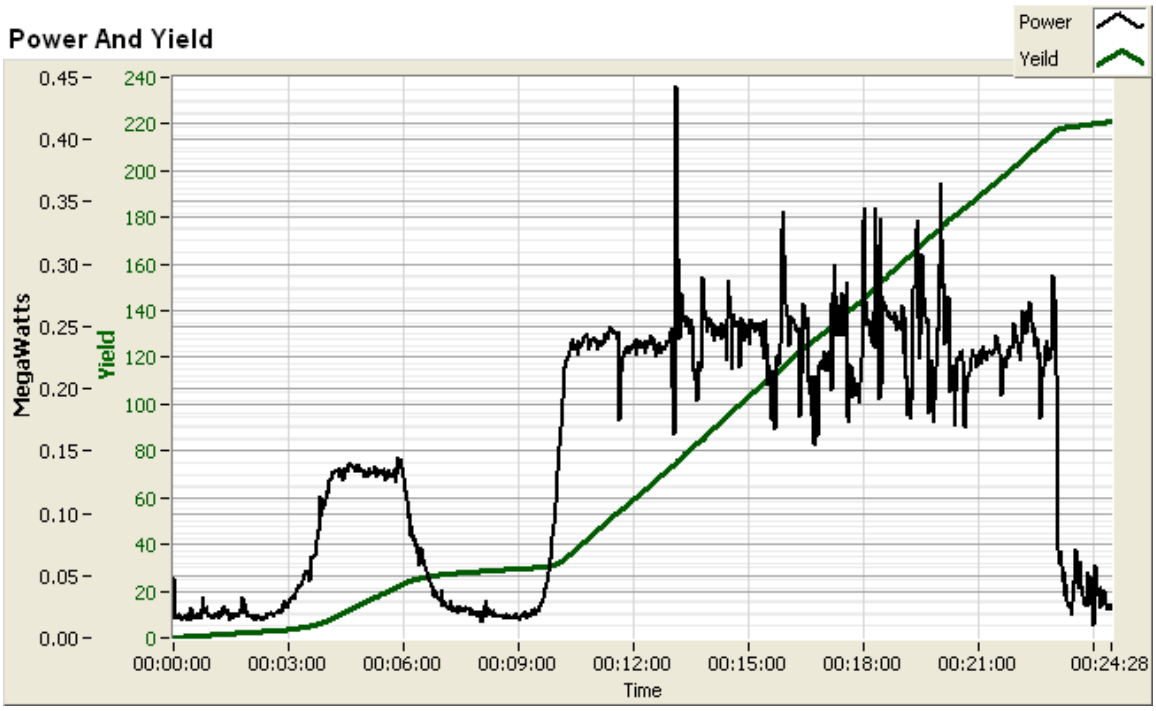

Figure 45. Power and Yield Data from the ACRR steady-state run.

There were four voltage measurements acquired from the test package during the ACRR steady-state test. Three thermocouples (TCs) and one strain gage provided insight to the test specimen's response to the neutron and photon fluxes in the central cavity. The initial "hump" in the strain gage data exhibited in Figure 46 occurs alongside the ramp-up to 5% of maximum reactor power. It should be noted that Figure 45 and Figure 46 have different time scales, because the reactor operators and experimenters were using separate time bases.

At the 9.5% steady-state power ramp, the strain gage shows increased values of strain, but then decreases before retaining a constant value of approximately 23 microstrain. However, this constant value of strain remains, even when the reactor power is decreased. This indicates a potentially damaged strain gage, because large values of strain are expected for a high radiation flux and smaller values are expected for low reactor power. When examining the data in Figure 46, it is helpful to use the shape of TC1 as analogous to reactor power, because this thermocouple was attached to the test specimen, which was located at the core centerline in the central cavity. TC2 was attached to one of the smaller, non-radiation hardened cameras located near the top of the test package. TC2's temperature is initially higher than that of TC1 due to the camera's internal heat generation. TC3 was located on the radiation-hardened camera, next to the TC2 camera at the top of the test package.

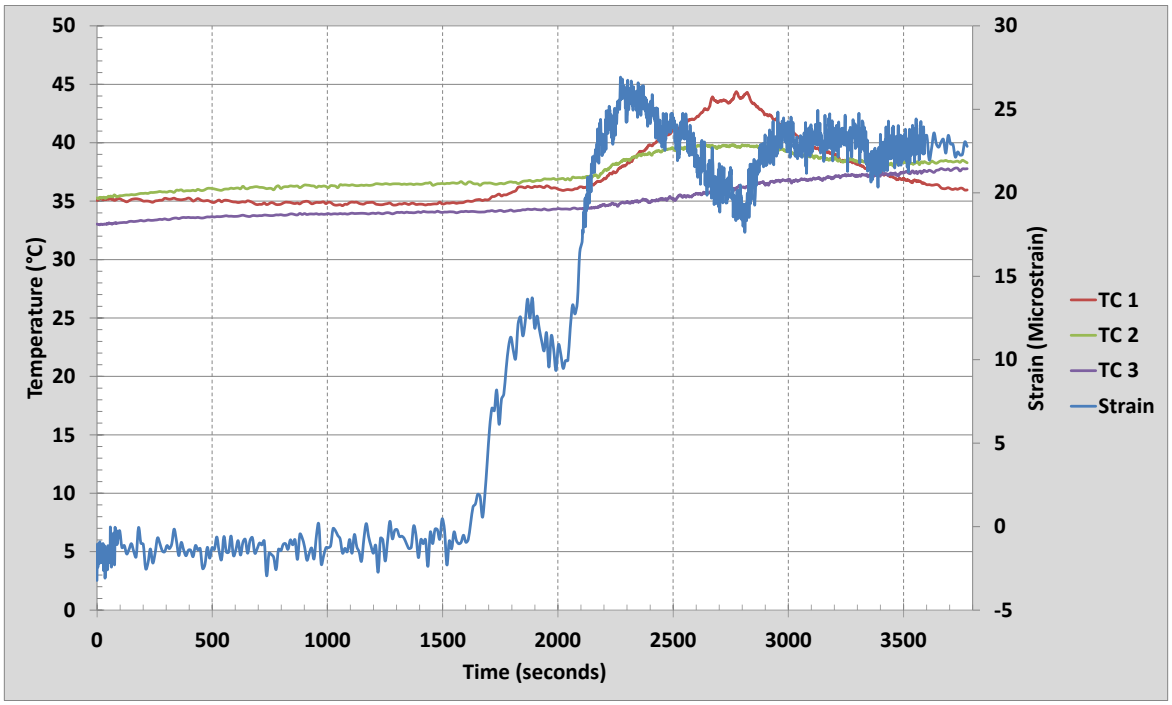

Figure 46. Strain and Temperature Measurements from ACRR test package.

As a result of the radiation in the ACRR central cavity during the test, it was suspected that there might be some damage to the camera and/or the lenses used in the borescope. The radiation-hardened camera seemed nominally functional at the shutdown of the reactor, despite the speckle "snow" effects during the experiment, as exhibited in Figure 44. Figure 47 through Figure 49 display the "yellowing" of the borescope lenses. The lens closest to the core centerline suffered the most discoloration. Also, there are two lenses in the center of Figure 48, meaning that each lens underwent approximately half of that discoloration.

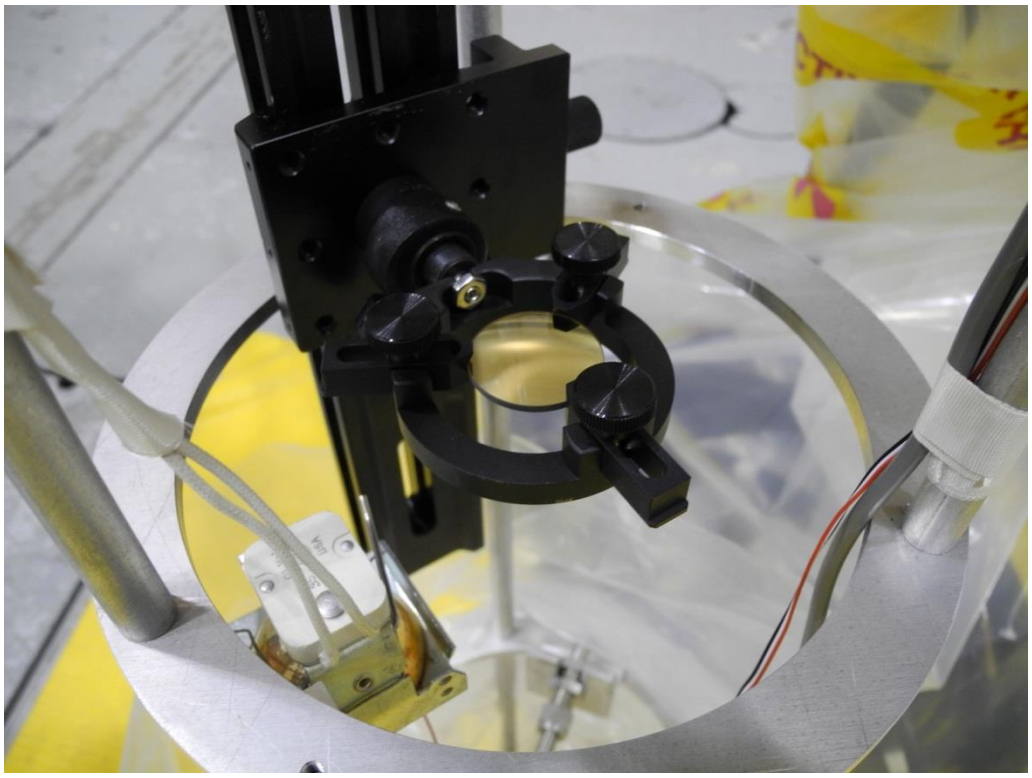

Figure 47. Lens closest to core centerline.

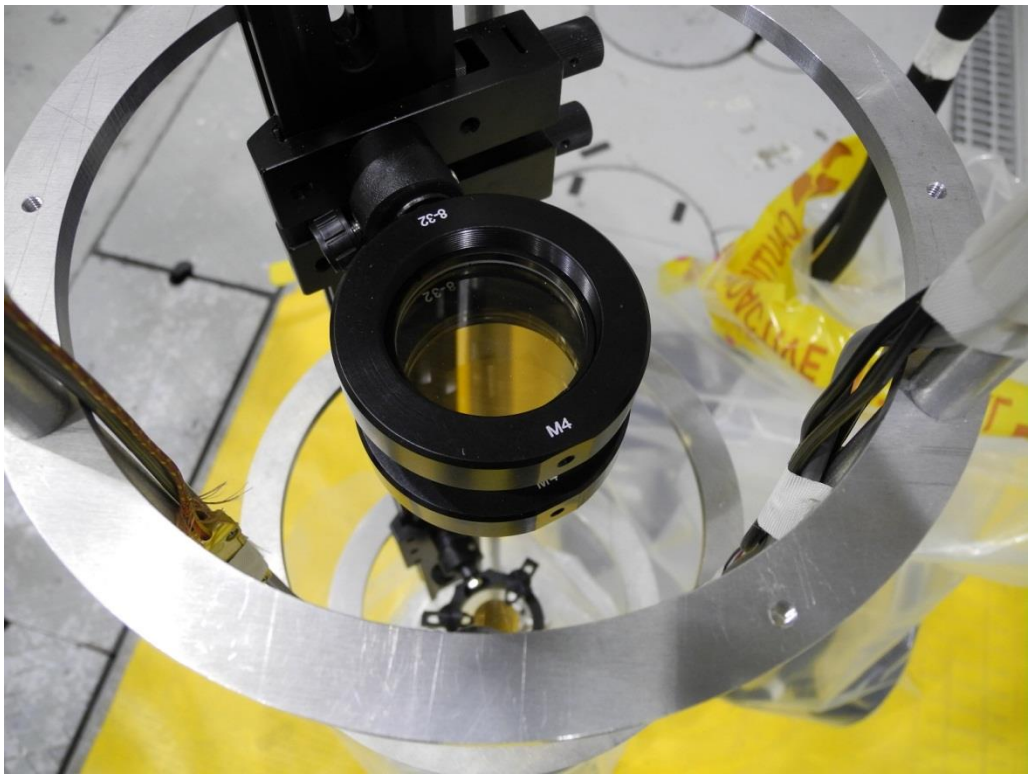

Figure 48. Mid-distance lenses. There are two in center of image.

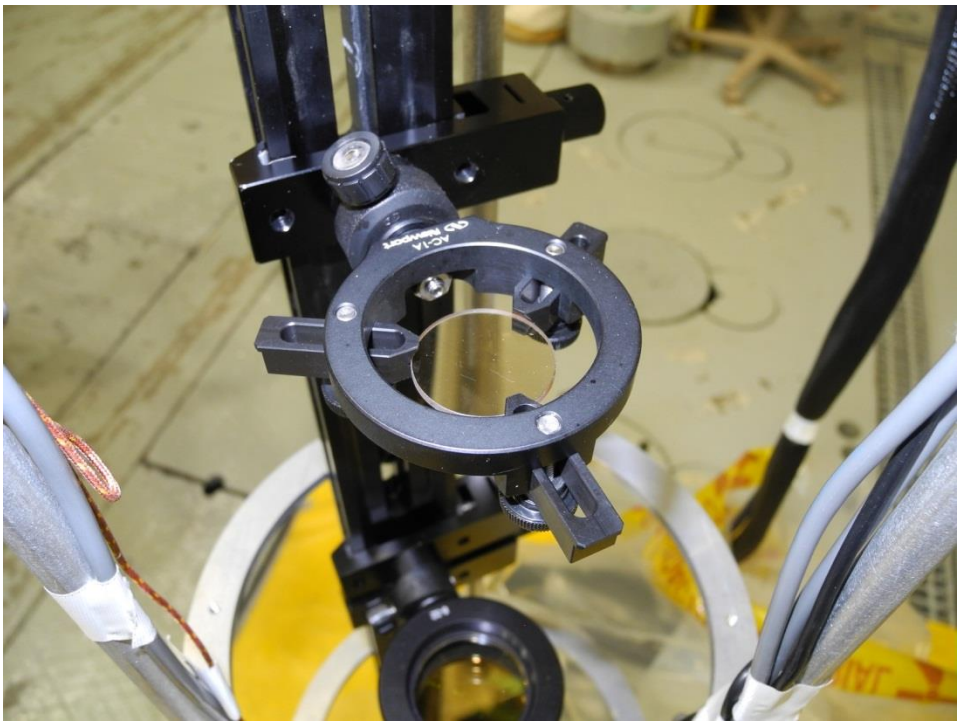

Figure 49. Lens farthest from core centerline.

Figure 50 provides a view of the bottom of the farthest lens from the core centerline. Also, the radiation-hardened camera, which was equipped with TC3, can be seen in the center of the image. Near the top of the image, one of the smaller, non-radiation hardened cameras can be seen. It was equipped with TC2 for measurements.

Figure 50. Bottom of farthest lens from core centerline.

9. CONCLUSIONS AND FUTURE WORK

The test on 14 August 2012 in ACRR provided several important qualitative baselines for the fuels testing LDRD program. Based on the two experiments in the reactor, it can be concluded that if strain measurements on fuel cladding are to be performed using resistive-type strain gages, then the test conditions will have to be stable, non-transient photon and neutron fluxes, and the strain gage installation to the cladding substrate must be exceptionally precise. If an optical approach is to be pursued, based on the uncertain results of the second ACRR experiment, then the photon flux to the camera must be substantially reduced to avoid "snow" on the camera image. In addition, any successful test set-up must be able to provide an ample light source for the camera.

For future ACRR tests for the LDRD, a larger scope lens will be attempted to increase the distance between the camera and the reactor core. Figure 51 shows the Celestron Spotting Scope, equipped with a 2000 mm lens. The camera portion of the optical instrument is the partially hidden black box with a bar code near the left side of the image.

The ACRR's central cavity is approximately thirty feet deep, creating the possibility that the equipment set-up in Figure 51 could be placed outside the central cavity, if it can successfully view the test specimen's speckle pattern to an accurate degree when placed at least thirty feet away.

Figure 52 is an image taken with the test set-up shown in Figure 51. The test specimen was placed approximately thirty feet away in an outdoor environment. The image could successfully be used to perform DIC and to calculate strain. This test set-up also successfully handled environmental issues, such as wind, humidity, and temperature effects. The distance of thirty feet is nominal to the 2000 mm lens. This lens can accurately view the speckle pattern of the test specimen at distances greater than fifty feet.

Figure 51. Celestron 2000mm Lens and Camera

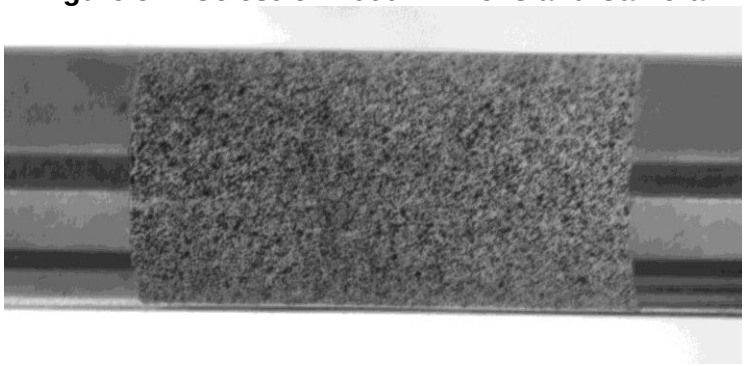

Figure 52. Image taken at a distance of thirty feet with Celestron 2000mm lens

Moving forward in this LDRD program, it is likely that by placing the camera, fitted with the 2000 mm lens, above the central cavity and observing the test specimen near the bottom of the cavity, the strain on the specimen due to a pulse could be quantified successfully.

10. REFERENCES

1. Hannah, R.L., Strain Gage User's Handbook. Chapman & Hall, London: 1992.

2. Young, Warren C., Budynas, Richard G., Roark's Formulas for Stress and Strain, 7th Edition. McGraw-Hill, New York: 2002.

THIS PAGE INTENTIONALLY LEFT BLANK

APPENDIX A – EQUATIONS

Basic Stress/Strain Relationship

Definition of Strain

$$\boldsymbol{\varepsilon = \frac{\delta}{L}} \tag{1}$$

Relationship between Stress and Strain (Hooke's Law)

$$\boldsymbol{\sigma = \varepsilon E} \tag{2}$$

Thin Wall

Derivation of Axial Stress -

Definition of stress (Force per unit area)

$$\boldsymbol{\sigma = \frac{F}{A}} \tag{3}$$

Area of wall needed to contain pressure

$$\boldsymbol{A = 2\pi r_m t} \tag{4}$$

$$\boldsymbol{\rightarrow F = 2\pi\sigma r_m t} \tag{5}$$

Force applied by the air volume's pressure on the cross-sectional area of the tube

$$\boldsymbol{F = PA_c = P(\pi r^2)} \tag{6}$$

$$\boldsymbol{\rightarrow P(\pi r^2) = 2\pi\sigma r_m t} \tag{7}$$

For a thin wall vessel, r_m can be assumed as r.

Axial (Longitudinal) Stress

$$\boldsymbol{\sigma_L = \frac{Pr}{2t}} \tag{8}$$

Derivation of Circumferential Stress -

Area of wall needed to contain pressure

$$\boldsymbol{A = 2Lt} \tag{9}$$

Force applied by the air volume's pressure on the cross-sectional area of the tube

$$\boldsymbol{F = PA_c = 2PLr} \tag{10}$$

$$\boldsymbol{\rightarrow 2PLr = 2\sigma Lt} \tag{11}$$

Circumferential (Hoop) Stress

$$\boldsymbol{\rightarrow \sigma_H = \frac{Pr}{t}} \tag{12}$$

Thick Wall

Definition of Axial Stress provided by Roark's Formulas for Stress and Strain

Eq. :

$$\boldsymbol{\sigma_L = \frac{P_i r_i^2}{r_o^2 - r_i^2}} \tag{13}$$

Definition of Hoop Stress provided by Roark's Formulas for Stress and Strain

Eq. :

$$\boldsymbol{\sigma_H = \frac{P_i r_i^2}{r_o^2 - r_i^2} - \frac{(P_o - P_i) r_i^2 r_o^2}{(r_o^2 - r_i^2) r^2}} \tag{14}$$

Definition of Axial Strain provided by Roark's Formulas for Stress and Strain

Eq. :

$$\boldsymbol{\varepsilon_L = \frac{\sigma_L - \upsilon \sigma_H}{E} + \alpha T} \tag{15}$$

Definition of Hoop Strain provided by Roark's Formulas for Stress and Strain

Eq. :

$$\boldsymbol{\varepsilon_H = \frac{\sigma_H - \upsilon \sigma_L}{E} + \alpha T} \tag{16}$$

During this set of experiments, the axial stress on the pipe is negligible due to manufacturing processes and other phenomenon, so:

Eq. :
$$|\boldsymbol{\varepsilon_L}| = \frac{\boldsymbol{\upsilon\sigma_H}}{\boldsymbol{E}} \tag{17}$$

Relationship between Hoop and Axial Strain is a function of Poisson's ratio (ν).

Eq. :
$$\frac{\boldsymbol{\varepsilon_H}}{\boldsymbol{\varepsilon_L}} = \frac{\boldsymbol{2-\upsilon}}{\boldsymbol{1-2\upsilon}} \tag{18}$$

When misaligning the strain gages by a certain angle on the pipe, the measured strain can be calculated, as well as the rate at which the strain changes with respect to its offset angle. ($\theta = 0°$ corresponds to pure hoop strain, while $\theta = 90°$ corresponds to pure axial strain):

$$\boldsymbol{\varepsilon_\theta} = \frac{\boldsymbol{1}}{\boldsymbol{2}}(\boldsymbol{\varepsilon_H - \varepsilon_L})(\boldsymbol{\cos 2\theta - 1}) + \boldsymbol{\varepsilon_H} = \boldsymbol{\varepsilon_H}\left(\boldsymbol{1} + \left(\frac{\boldsymbol{1+\nu}}{\boldsymbol{4-2\nu}}\right)(\boldsymbol{\cos 2\theta - 1})\right) \tag{19}$$

$$\frac{\boldsymbol{d\varepsilon_\theta}}{\boldsymbol{d\theta}} = (\boldsymbol{\varepsilon_L - \varepsilon_H})\,\boldsymbol{\sin 2\theta} \tag{20}$$

The Gage Factor (GF) is a property of a strain gage that relates a change in resistance ($\boldsymbol{\Delta R/R}$) to strain in the substrate material.

$$\boldsymbol{\varepsilon} = \frac{\boldsymbol{\Delta R/R}}{\boldsymbol{GF}} \tag{21}$$

Distribution

1e	MS0771	Andrew Orrell	6200
1e	MS0736	Tito Bonano	6220
3	MS1130	Aaron Hall	1832
3	MS1130	David Urrea	1832
1e	MS1136	Gary Rochau	6221
1e	MS1136	David Ames	6221
1e	MS1136	Tom Conboy	6221
3	MS1136	Darryn Fleming	6221
3	MS1136	Thomas Holschuh	6221
1e	MS1136	Tom Lewis	6221
1e	MS1136	Bob Moore	6221
3	MS1136	Ed Parma	6221
3	MS1139	Tim Miller	1535
1e	MS0899	Technical Library	9536
1e	MS0359	D. Chavez, LDRD Office	1911

THIS PAGE INTENTIONALLY LEFT BLANK


Sandia National Laboratories